RSC Advances

PAPER

View Article Online
View Journal | View Issue

Cite this: *RSC Adv.*, 2025, **15**, 33916

Synergistic catalytic activation of persulfate by $CuMnO_2$–CoPc heterostructures on Ti foam: kinetics and mechanism of antibiotic oxidation

Dinh Ngo Vu,[a] Van Chau Dinh,[a] Tien Hoang Nguyen,[b] Thi Thao Minh,[a] Phuoc Cuong Le,[c] Tan Nhat*[de] and Dinh Nhi Bui*[a]

Received 30th July 2025
Accepted 27th August 2025

DOI: 10.1039/d5ra05544j

rsc.li/rsc-advances

This study presents a novel heterogeneous catalyst system – $CuMnO_2$@cobalt phthalocyanine immobilized on titanium foam ($CuMnO_2$@CoPc/Ti foam) – that is highly effective in treating three common antibiotics, ofloxacin (OFL), levofloxacin (LEVO) and sulfanilamide (SFA), through UV-persulfate-based advanced oxidation (UV/PS). Comprehensive characterization (XRD, SEM-EDS, FTIR, BET, XPS, and UV-vis DRS) confirms a stable mesoporous architecture and uniform coating; the specific surface area increases from 55.3 to 60.8 $m^2\ g^{-1}$ after CoPc deposition, and the apparent optical band gap narrows from ≈1.41 to ≈1.31 eV, indicating improved visible-light response. Antibiotic decay follows pseudo-first-order kinetics with k_{app} of 0.0426 ± 0.0015, 0.0410 ± 0.0017, and 0.0393 ± 0.0013 min^{-1} for OFL, LEVO, and SFA, respectively, delivering >90% removal in 60 min. TOC mineralization reaches ≈69–72%, evidencing deep oxidation beyond parent-compound loss. Mechanistically, XPS verifies persistent Cu^{2+}/Cu^{+} and Mn^{4+}/Mn^{3+} surface couples (Co states stable), while EPR with DMPO detects $SO_4^{\bullet-}$ and $^{\bullet}OH$, with sulfate radicals dominating. The monolithic catalyst is reusable over 5 cycles with negligible activity loss and ultra-low metal leaching (Cu/Mn/Co ≪ 0.1 mg L^{-1} by ICP-OES), underscoring chemical robustness. These results highlight $CuMnO_2$@CoPc/Ti foam as a durable, separable platform for UV/PS treatment of antibiotic-bearing waters and provide a mechanistic blueprint—combining photosensitization and multi-center redox—to guide future reactor-scale implementations.

1 Introduction

In recent years, the increasing presence of emerging contaminants, especially antibiotics such as ofloxacin, levofloxacin, and sulfanilamide, has become a serious threat to aquatic environments and ecosystems.[1,2] Even at very low concentrations (ng/L), antibiotics are able to trigger antimicrobial resistance (AMR) and disrupt ecosystems.[3] Traditional treatment methods such as biological treatment, adsorption, and chlorination often cannot completely degrade the complex molecular structures of these substances, leading to residual leakage into the effluent and increasing public health risks.[4–6]

Meanwhile, Advanced Oxidation Processes (AOPs) technologies based on the generation of strong oxidizing radicals ($SO_4^{\bullet-}$, $^{\bullet}OH$) have attracted attention due to their ability to thoroughly treat difficult-to-degrade organic compounds such as antibiotics.[7–10] The UV/PS method – activating persulfate with ultraviolet light – is particularly notable for its higher oxidation efficiency compared to UV/H_2O_2 or ozonation, due to the generation of both sulfate radicals and hydroxyl radicals.[11,12] The UV/PS system has demonstrated the effectiveness of removing antibiotics such as ciprofloxacin, sulfamethoxazole with a fast reaction rate and the ability to operate under neutral pH conditions.[13,14]

However, the actual efficiency of the UV/PS system depends greatly on the structure and properties of the catalyst. In many recent studies, the development of heterostructure catalysts has shown the ability to effectively control the electron flow, reduce electron–hole recombination, and enhance the conversion of PS to $SO_4^{\bullet-}$ radicals through active metal redox pairs.[15–17] $CuMnO_2$ is a mixed oxide of Cu and Mn, so they have the ability to enhance acid and base resistance, increase surface area and strengthen catalytic stability compared to single metal oxides.[18,19] The induction of $CuMnO_2$ when interacting with PS under UV light leads to continuous peroxo activation, increased $SO_4^{\bullet-}$ generation through the conversion of Cu(II)/Cu(I) and Mn(III)/Mn(II).[20,21] A study by Chen *et al.*[22] demonstrated that nano-$CuMnO_2$ when combined with PS could remove up to 93%

[a]*Electric Power University, Ha Noi, Vietnam. E-mail: vietnamkz@yahoo.com*
[b]*The University of Danang, University of Science and Education, 459 Ton Duc Thang st., Da Nang 550000, Vietnam*
[c]*The University of Danang, University of Science and Technology, Danang, 550000, Vietnam*
[d]*Institute of Research and Development, Duy Tan University, Da Nang, Vietnam. E-mail: ttnhat@duytan.edu.vn*
[e]*School of Medicine and Pharmacy, Duy Tan University, Da Nang, Vietnam*

of orange I in just 30 min of reaction, while the efficiency of $CuMnO_2$ alone was significantly lower (below 50%).

The surface of $CuMnO_2$ when coated with cobalt phthalocyanine (CoPc) (*via* π–π connection) forms a heterogeneous catalyst system $CuMnO_2$@CoPc, expanding the surface area, providing more active sites and enhancing the interaction with PS and UV light. Several similar studies have applied the combination of different materials with CoPc to increase the efficiency of environmental pollution treatment. For example, in the photocatalytic study of MB degradation, Fe_3O_4@SiO_2@-TiO_2@CoPcS microspheres showed significantly higher activity (86.4%) than Fe_3O_4@SiO_2@TiO_2 microspheres (<60%).[23] Another study on CoPcTs/TiO_2 showed that coating phthalocyanine on the TiO_2 surface improved the degradation efficiency of thionine dye significantly compared to the original TiO_2 (degradation efficiency of 90% for CoPcTs/TiO_2 and 40% for TiO_2 after 120 min of treatment).[24] However, these systems still have limitations such as the influence of pH, electron–hole recombination rate and suboptimal efficiency when treating different antibiotic mixtures.

To ensure mechanical strength and easy recovery, $CuMnO_2$@CoPc is immobilized on titanium foam (Ti foam). Titanium foam not only has good resistance to corrosive environments and has a 3D porous structure, but also has effective surface interaction with thin catalyst layers, supporting reusability and reducing catalyst loss.[25–27]

To date, there have been only a limited number of studies combining $CuMnO_2$ and CoPc heterostructures in metal foam structures. However, similar catalytic systems such as MIL 101(Fe)/MoS_2, Cu@MoS_2/PAAm/CA NCDN, g-C_3N_4/Mn_3O_4/ZIF-8 have provided clear evidence of the ability to enhance the photolysis and PS conversion efficiency in the presence of asymmetric electron pairs and multi-component heterostructures.[28–30] In particular, the MIL 101(Fe)/MoS_2/PS system has a much faster degradation rate of tetracycline (85% in 40 min) than each individual component, while g-C_3N_4/Mn_3O_4/ZIF-8/PMS gives rhodamine B (RhB) degradation efficiency up to >96% and the efficiency does not change much (decrease 1.7%) after 5 cycles of use – a remarkable achievement for the development of new generation heterostructures.

Several recent studies have demonstrated that foam-encapsulated heterojunction catalysts have superior performance. For example, hierarchical porous N–TiO_2/carbon foam composite demonstrated impressive performance, this material is capable of removing 97% of phenol within 2 hours under simulated sunlight irradiation and its photocatalytic activity is 4.9 times higher than that of N–TiO_2 and 10.8 times higher than that of pure TiO_2, confirming its superiority in applications related to pollutant degradation.[31] Another study on Ti-foam/TiO_xH_y–NTs/SnO_2–Sb showed that this material exhibited excellent ability in effectively decomposing the real and simulated PAM-containing fracturing flowback fluid, achieving a chemical oxygen demand degradation of over 90.0% after 120 min of EO process.[32]

The expectation of this study is to demonstrate that $CuMnO_2$@CoPc/Ti foam when combined with UV/PS will bring superior antibiotic treatment efficiency, high material durability and practical application in wastewater treatment plants.

2 Experiment

2.1. Synthesis of $CuMnO_2$@CoPc/Ti foam

$CuMnO_2$ was synthesized by ultrasound-assisted co-precipitation.[33] Initially, the precursor salts $Cu(NO_3)_2 \cdot 3H_2O$ and $Mn(NO_3)_2 \cdot 4H_2O$ were separately dissolved in 20 mL of distilled water according to the prescribed chemical ratio. After mixing the two solutions and stirring on a magnetic stirrer for 10 min, 40 mL of 2.5 M NaOH solution was slowly added to form a precipitate while continuing to stir. The resulting precipitate was then treated by ultrasonic vibration for 30 min at 80 °C, using an ultrasonic processor "Sonics Vibra Cell VCX-750" at a frequency of 20 kHz. Finally, the precipitate was separated by decantation, filtration and repeated washing with distilled water on filter paper until reaching neutral pH. The material was then dried in air, in an oven at 80 °C for about 4 h to complete the synthesis.

After obtaining the dry $CuMnO_2$, about 0.2 g of the material was dispersed in 50 mL of ethanol containing 0.05 g of CoPc. The mixture was ultrasonicated for 2 h to ensure the π–π interaction between the phthalocyanine rings and the metal oxide surface. This process was to form the $CuMnO_2$@CoPc heterojunction, which helps to expand the surface area and provide more active catalytic sites. Finally, the material was filtered, gently dried at 60 °C, and a characteristic dark blue powder was obtained.

The Ti foam was cut into 2 cm × 2 cm pieces and soaked in 0.1 M HCl solution under ultrasonication for 15 min to clean the surface and enhance adhesion. After rinsing with distilled water and ethanol, the Ti foam was dried and immersed in a solution containing $CuMnO_2$@CoPc dispersed in ethanol. The immersion-heat system was repeated 3 times, each immersion was followed by a drying at 80–100 °C for 1 hour. The catalyst layer was formed stably and firmly adhered to the surface of the Titan foam, forming a $CuMnO_2$@CoPc/Ti foam system ready for the photocatalytic process.

2.2. UV/PS photochemical reaction system setup

The antibiotic degradation reaction was carried out in a reaction system consisting of a 15 W UV lamp (wavelength 254 nm) fixed above a glass reaction beaker. The distance between the lamp and the solution surface was 5 cm. Each experiment used 200 mL of antibiotic solution (ofloxacin, levofloxacin or sulfanilamide) with an initial concentration of 10 mg L^{-1}. The persulfate (PS) concentration was kept constant at 2.0 mM. The reaction solution had an initial pH of 4, and was stirred continuously at 300 rpm during the 60-minute UV irradiation. The temperature was kept constant at 30 °C and the mass of catalyst introduced was 0.4 g L^{-1}. At 0, 10, 20, 30, 45 and 60 minutes, 5 mL of sample was taken out, filtered through a 0.22 μm membrane and stored at 4 °C for analysis of the remaining antibiotic concentration.

Antibiotic concentrations were measured by LC-MS/MS analysis,[34] while the extent of mineralization was assessed using TOC. In addition, the role of free radicals $^{\bullet}OH$ and $SO_4^{\bullet-}$ in the degradation mechanism was clarified by radical scavenging experiments using ethanol and *tert*-butanol.

2.3. Catalyst characterization

The $CuMnO_2$@CoPc/Ti foam catalyst was characterized by various analytical techniques to determine the crystal structure, surface morphology, elemental composition, chemical bonding and thermal properties. The surface morphology and particle size of the material were examined by scanning electron microscopy (SEM) combined with energy dispersive X-ray spectroscopy (EDS) to evaluate the elemental distribution. The sample was coated with a thin conductive Pt layer before being placed in the SEM chamber. The crystal structure of the material was determined by X-ray diffraction (XRD) using an XRD device with Cu Kα radiation ($\lambda = 1.5406$ Å), scanning in the 2θ range from 5° to 70°. The characteristic chemical functional groups and molecular interactions in the material were analyzed by Fourier Transform Infrared Spectroscopy (FTIR) in the wavelength range from 4000 to 400 cm^{-1}. The specific surface area and capillary volume were determined by nitrogen adsorption–desorption method (BET analysis – Brunauer–Emmett–Teller). The sample was degassed at 120 °C for 6 hours before measurement on an automatic BET instrument. The thermal stability of the material was investigated by thermogravimetric analysis (TGA) in air, at a temperature range from room temperature to 800 °C, with a heating rate of 10 °C min^{-1}. The sample mass was about 5–10 mg, placed in a platinum sample pot. XPS measurements with Al Kα source ($h\nu = 1486.6$ eV), vacuum < 1×10^{-8} mbar; charge neutralization when necessary. High-resolution spectra (Cu 2p, Mn 2p, Co 2p, O 1s): pass energy 20 eV, step 0.05 eV, accumulation ≥ 5 times. Charge calibration to C 1s = 284.8 eV. CasaXPS processing: Shirley background, GL-mix peak 30–40%, spin–orbit constraint to standard; satellites modeled but not included in valence %. X-band EPR (≈9.84 GHz, CW mode) was performed at 298 K with a flat quartz tube; microwave power 20 mW, modulation 100 kHz, amplitude 1.0 G, 100 G scan around $g = 2.00$, accumulation 4–6 times/spectrum; g was standardized with Mn^{2+} and relative intensity was quantified by quadratic integration. The reaction system consisted of 10 mg per L antibiotic, 2.0 mM persulfate (PS), 0.30 g per L $CuMnO_2$@CoPc/Ti foam catalyst and 50 mM DMPO trapping agent; UV irradiation was similar to the decomposition experiment and the sample was withdrawn 30–60 s after UV turn-on. $^{\bullet}OH$ identification was performed in H_2O (1 : 2 : 2 : 1 quartet, $g \approx 2.005$), and $SO_4^{\bullet-}$ in a 50% v/v MeOH/H_2O mixture to stabilize the DMPO–$SO_4^{\bullet-}$ adduct (6-line model, $g \approx 2.006$). Controls included no UV, no PS, and no catalyst; parallel radical quenching experiments with EPR using 0.5 M *tert*-butanol (quenching $^{\bullet}OH$), 1.0 M MeOH (quenching both $SO_4^{\bullet-}$/$^{\bullet}OH$), and 20 mM NaN_3 (quenching $^1O_2$). Each condition had $n = 3$ replicates and the mean ± SD was reported.

2.4. Reusability and stability testing

The reusability and durability of the $CuMnO_2$@CoPc/Ti foam catalyst were evaluated through successive treatment cycles. After each reaction cycle, the catalyst was removed from the solution, the catalyst was washed with distilled water and ethanol to remove impurities or intermediate products on the surface, and then dried at 60 °C for 2 h before being used for the next cycle, the solution was acidified with 2% HNO_3 and quantified by ICP-OES. Quantification was performed using external calibration (0–100 μg L^{-1}) prepared in 2% HNO_3; linearity $R^2 \geq 0.999$ for all analytes. Analytical wavelengths were selected to minimize spectral overlap (Cu 324.754 nm; Mn 257.610 nm; Co 228.616 nm) with on-peak/adjacent-peak background correction. Procedural blanks and a catalyst-free reaction blank were included each batch. The method LOD/LOQ were ~1/3 μg L^{-1} (*i.e.*, 0.001/0.003 mg L^{-1}) for Cu, Mn and Co. A total of 5 cycles were conducted under the same reaction conditions: initial pollutant concentration of 10 mg L^{-1}, persulfate concentration of 2.0 mM, UV irradiation time of 60 min, and catalyst mass of 0.3 g L^{-1}.

The treatment efficiency was evaluated by measuring the remaining pollutant concentration in the solution after the reaction using LC-MS/MS, and determining the degree of mineralization through analysis of total organic carbon (TOC).

$$H(\%) = \frac{C_0 - C_t}{C_0} \times 100\%$$

where H is the treatment efficiency (%); C_0 is the initial antibiotic concentration, mg L^{-1}; C_t is the antibiotic concentration at time t, mg L^{-1}.

$$\text{Degree of mineralization}(\%) = \frac{\text{TOC}_0 - \text{TOC}_t}{\text{TOC}_0} \times 100\%$$

where TOC_0 is the initial TOC and TOC_t is the TOC at time t.

To evaluate the stability of the catalyst after cycles of use, the surface morphology and elemental composition were re-analyzed by SEM-EDS.

3 Results and discussion

3.1. Characteristics of $CuMnO_2$@CoPc/Ti foam catalyst

Fig. 1 shows the X-ray diffraction patterns of three samples of $CuMnO_2$, $CuMnO_2$@CoPc, CoPc, Ti foam and $CuMnO_2$@CoPc immobilized on Titan foam. For the $CuMnO_2$ sample, the diffraction peaks at $2\theta \approx 15.6°$, 31.5°, 33.6°, 35.5°, 37.1°, 40.8°, 52.8°, 57.3°, 59.5°, 60.0°, and 65.1° correspond to the (001), (002), (200), (110), (11−1), (111), (202), (11−3), (31−1), and (004) crystal planes of the $CuMnO_2$ phase (JCPDS 50-0860). These peaks confirm that the $CuMnO_2$ material was successfully synthesized in a well-crystalline form, consistent with the report of Cuixia Cheng[35] when synthesizing $CuMnO_2$ by hydrothermal method.

After CoPc coating, some XRD peaks of $CuMnO_2$ tended to weaken and broaden, especially at 30–40°, indicating the presence of an organic coating on the metal oxide surface. The $CuMnO_2$@CoPc/Ti foam sample still retains the diffraction characteristics of $CuMnO_2$, while the peaks at 38.4°, 40.1° and 53.2° are attributed to the crystal structure of Titan foam.[36] The absence of significant XRD peak shift after CoPc attachment indicates that the π–π interaction between CoPc and $CuMnO_2$ does not alter the oxide crystal structure, which helps preserve the electronic properties of the catalyst matrix.

The scanning electron microscopy (SEM) image in Fig. 2 shows that $CuMnO_2$ has a nano-sized particle morphology. The

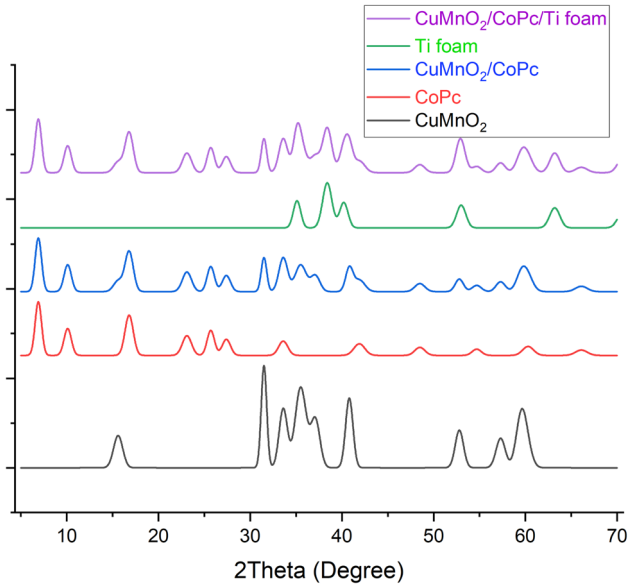

Fig. 1 XRD spectra of the studied samples.

morphological data from scanning electron microscopy (SEM) provide clear evidence of the nanostructure of the material. The $CuMnO_2$ sample exhibits a discrete, uniformly distributed bulk morphology with a particle size ranging from 50 to 100 nm. After CoPc coating, the particle surface becomes rough and has an uneven thin film coating, which is typical of the phenomenon of organic material coating on metal oxides. When observing the $CuMnO_2$@CoPc sample fixed on the Titan foam, the adhesion of the catalyst layer to the three-dimensional porous structure of the Ti foam matrix can be clearly seen. This porous structure acts as a mechanical support, both facilitating the surface reaction and allowing the efficient flow of the solution through – which recent study with graphite/TiO_2/nickel foam has also exploited to improve the photocatalytic efficiency in continuous flow systems.[37]

Elemental composition analysis by EDS (Fig. 3) showed the simultaneous presence of Cu, Mn, Co, O and Ti elements with a Cu : Mn mass ratio of nearly 1 : 1, reaffirming the mixed oxide structure of $CuMnO_2$. The Co content is about 2.4 wt%, which is equivalent to the appropriate CoPc coverage level for the catalytic reaction without blocking the active sites. Many studies showed that too high a capping agent content can reduce the contact between the catalyst and the oxidizing agent, reducing the overall performance.[38]

The FT IR spectrum obtained for the $CuMnO_2$@CoPc/Ti foam material clearly shows the characteristic absorption bands for each component (Fig. 4). The broad absorption band at around 3450 cm^{-1} is due to the stretching vibration of the –

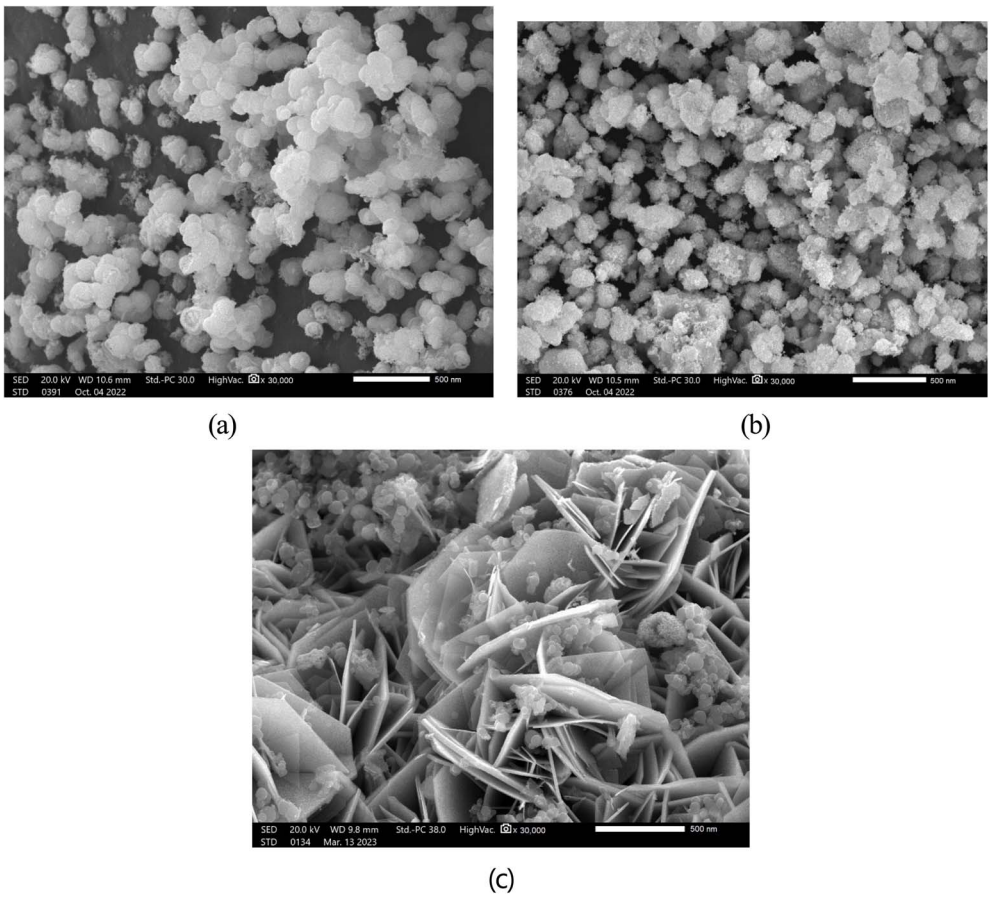

Fig. 2 SEM images of the surface of $CuMnO_2$ (a), $CuMnO_2$@CoPc (b), and $CuMnO_2$@CoPc/Ti foam (c).

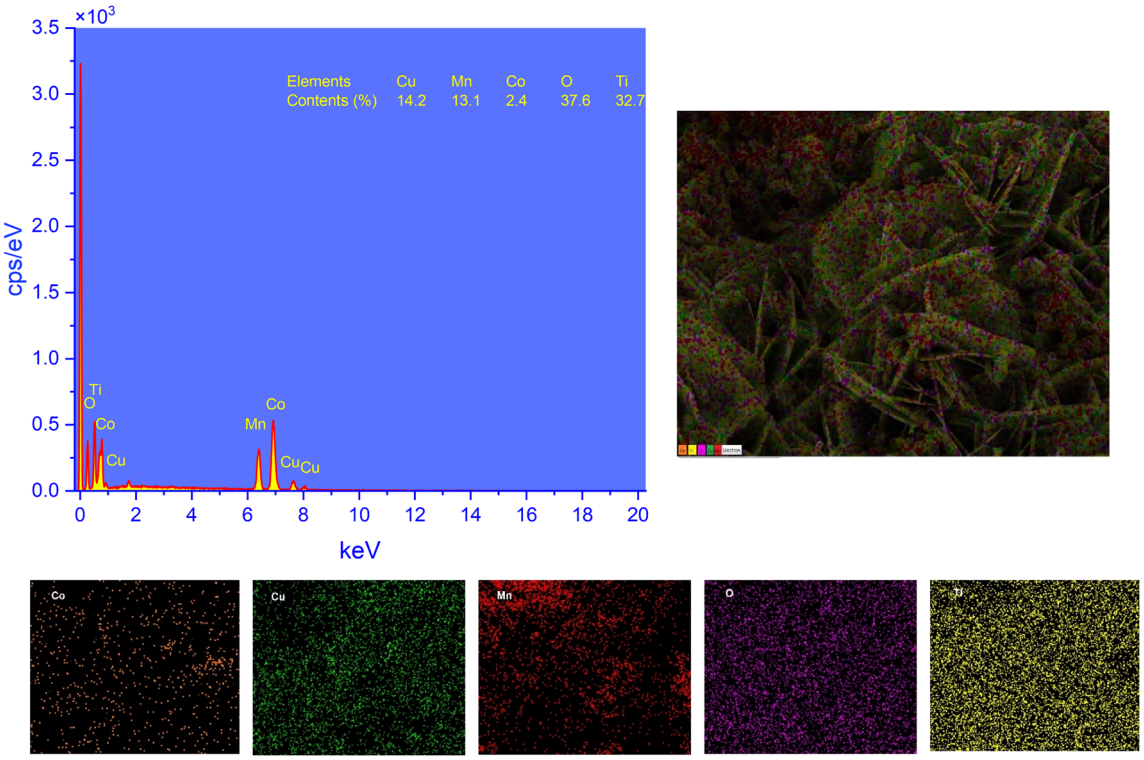

Fig. 3 Elemental distribution for $CuMnO_2$@CoPc/Ti foam.

OH group and the presence of adsorbed water on the oxide surface, which is a common feature in oxide-based catalysts. The bands at around 1330 cm^{-1} are assigned to the C–C/C–N stretching vibrations in the phthalocyanine ring, while the peak at 723 cm^{-1} is the out-of-plane C–H vibration characteristic of the α phase of phthalocyanine. The region of 500–700 cm^{-1} shows two weak peaks at 625 cm^{-1} and 515 cm^{-1}, corresponding to the stretching vibrations of Mn–O and Cu–O in the mixed oxide. Compared with the FT IR spectrum of pure Cu doped Mn_3O_4/Mn doped CuO, the metal–oxygen peaks in the $CuMnO_2$@CoPc sample have significantly lower intensities,[39] which reflects the coverage of the CoPc layer on the oxide surface, which attenuates the lattice vibration signal. This result is consistent with the report on NiO/CoPc materials by Sheena

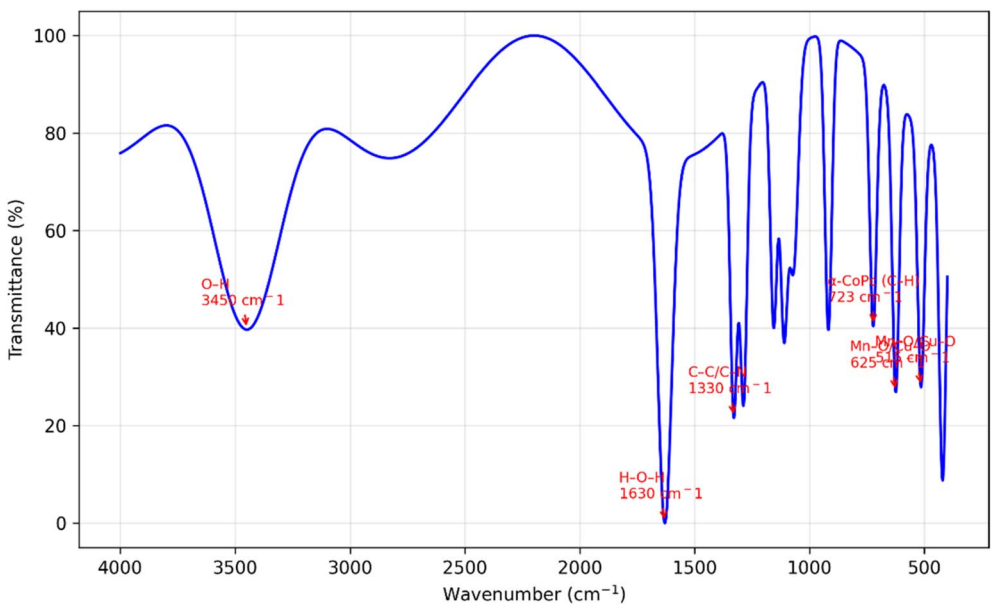

Fig. 4 FTIR spectra of $CuMnO_2$ and $CuMnO_2$@CoPc/Ti foam.

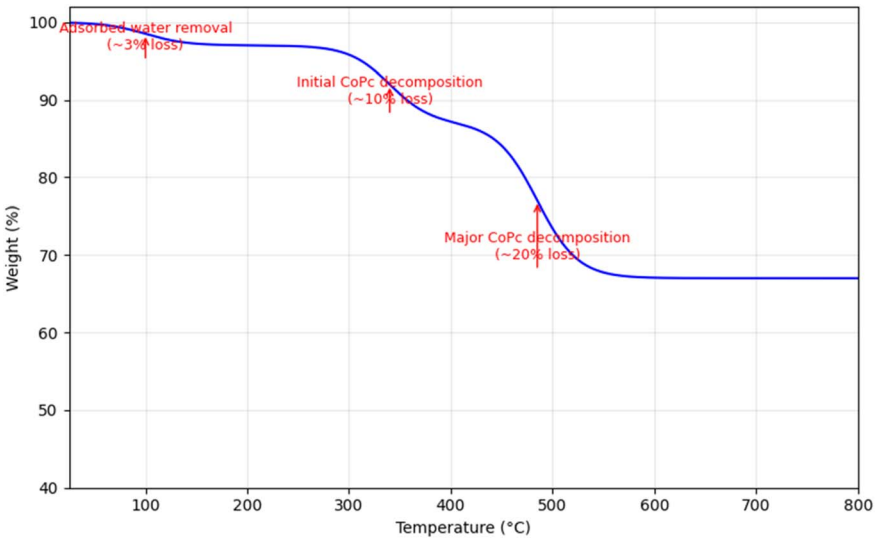

Fig. 5 TGA curves of $CuMnO_2$@CoPc/Ti foam.

et al., in which the characteristic vibrational bands of CoPc such as 1330, 1287, 1156, and 723 cm^{-1} are preserved when CoPc is covered on the oxide.[40] Thus, the FT IR spectrum of $CuMnO_2$@CoPc/Ti foam both confirms the presence of the phthalocyanine layer through characteristic vibrational bands, and shows that this coating weakens the metal–oxygen vibrations, demonstrating the interaction between the CoPc layer and the oxide substrate – a phenomenon that has also been observed in other oxide-coated phthalocyanine material systems.

The thermal stability of the catalyst was evaluated by thermogravimetric analysis (TGA) in air (Fig. 5). The TGA spectrum of $CuMnO_2$@CoPc/Ti foam shows three distinct mass loss stages when heated from room temperature to 800 °C. In the first stage, the sample lost about 3% of its mass below 150 °C, mainly due to the evaporation of water and the removal of hydroxyl groups adsorbed on the oxide surface. This is a common phenomenon for many oxide materials, and the small mass loss confirms that the sample was well dried before the measurement. When the temperature increased to the 300–380 °C region, the mass continued to decrease by about 10%. This loss was attributed to the initial decomposition of the phthalocyanine layer. Our results are consistent with the study of substituted metal phthalocyanines, where TGA showed that CoPc and CuPc started to lose mass at 300–309 °C.[41] The organic functional groups on the phthalocyanine decompose first, leading to a decrease in initial mass but the macrocyclic structure remains. The strongest mass loss occurs in the range of 420–550 °C, with a loss of about 20% of the initial mass. This stage corresponds to the complete decomposition of the phthalocyanine ring into inorganic products such as cobalt oxide. In the study of the CoPc/hybrid carbon system, the derivative TGA curve of CoPc shows only one decomposition peak with an onset around 440 °C,[42] which is consistent with the strong mass loss in our sample. After the loss of most of the organic component, the TGA curve becomes flat – the mass is stable up to 800 °C. This indicates that the $CuMnO_2$ framework and the Ti foam layer are thermally stable; In fact, studies on $CuMnO_2$ show that this material does not decompose but even absorbs oxygen, leading to an increase in mass when calcined in an oxidizing environment.[43] Compared with other works, the mass loss of $CuMnO_2$@CoPc/Ti foam is smaller than that of $CuMnO_2$@CoPc without Ti foam matrix (usually losing 30–40% of mass), due to the large mass fraction of Ti foam matrix reducing the proportion of CoPc in the whole material. At the same time, the observed decomposition temperatures (~300 °C and 440–500 °C) coincide with the decomposition milestones recorded for CoPc and its derivatives, indicating that the coating of CoPc onto $CuMnO_2$ did not significantly change the pyrolysis behavior of phthalocyanine. The TGA spectra also confirmed that after the decomposition of CoPc, the $CuMnO_2$ framework and Ti foam remained stable, similar to previous reports on the thermal stability of $CuMnO_2$.

The BET results show a clear difference in surface area and pore volume between the materials (Table 1). The pure $CuMnO_2$ sample has a surface area of 55.3 $m^2\ g^{-1}$ and a pore volume of 0.25 $cm^3\ g^{-1}$, this value is very close to the 54.9 $m^2\ g^{-1}$ previously reported for $CuMnO_2$/NF[44] and is within the usual range for mesoporous transition oxides. When cobalt phthalocyanine is added, the surface area increases slightly to 60.8 $m^2\ g^{-1}$ and the pore volume to 0.30 $cm^3\ g^{-1}$. This increase is consistent with the trend observed in similar material systems: in the $CuMnO_2$–rGO nanocomposite, the voids between the rGO and the

Table 1 BET measurement results

Samples	Surface area ($m^2\ g^{-1}$)	Capillary volume ($cm^3\ g^{-1}$)
$CuMnO_2$	55.3	0.25
$CuMnO_2$@CoPc	60.8	0.3
$CuMnO_2$@CoPc/Ti foam	20.4	0.14

$CuMnO_2$ nanoplates increased the surface area from 54.9 to 90.3 $m^2\ g^{-1}$, and in the CoPc/Ti_3C_2 system, the CoPc layer increased the SBET from 118.5 to 126.1 $m^2\ g^{-1}$.[45] These studies show that introducing an organic phase into the oxide framework can create new pores or expand the diffusion channel without clogging the existing micropores. Compared to the gCN system, in which $CuMnO_2$-gCN achieved a surface area of 82.29 $m^2\ g^{-1}$ and a pore volume of 0.429886 $cm^3\ g^{-1}$,[46] the CoPc layer produced a more moderate increase – perhaps because the bulky structure of phthalocyanine did not create a pore network as large as gCN. However, when the $CuMnO_2$@CoPc material was anchored onto the titanium foam framework, the surface area and pore volume decreased sharply to 20.4 $m^2\ g^{-1}$ and 0.14 $cm^3\ g^{-1}$, respectively. This decrease reflects the influence of the large mass fraction and low surface area of the Ti foam. The Ti foam matrix itself has a surface area of only 0.055–0.12 $m^2\ g^{-1}$,[47] when coated with the active material, the specific surface area of the entire composite is diluted by the foam mass. This result emphasizes that compared to light matrices such as gCN or rGO, the presence of a heavy metal matrix will significantly reduce the surface area per unit mass, thereby affecting the catalytic activity of the material.

3.2. Degradation efficiency of antibiotics

3.2.1. Reaction kinetic analysis. To clarify the degradation mechanism of three representative antibiotics – ofloxacin (OFL), levofloxacin (LEVO) and sulfanilamide (SFA) – by $CuMnO_2$@CoPc/Ti foam combined with UV/PS, three assumed kinetic models including zero-order, first-order and second-order were applied. The concentration data were processed to construct the corresponding plots: C *vs.* t (zero-order), $\ln(C)$ *vs.* t (first-order) and $1/C$ *vs.* t (second-order). The linear correlation coefficients R^2 were used to evaluate the suitability of each model. The results showed that the assumed first-order kinetic

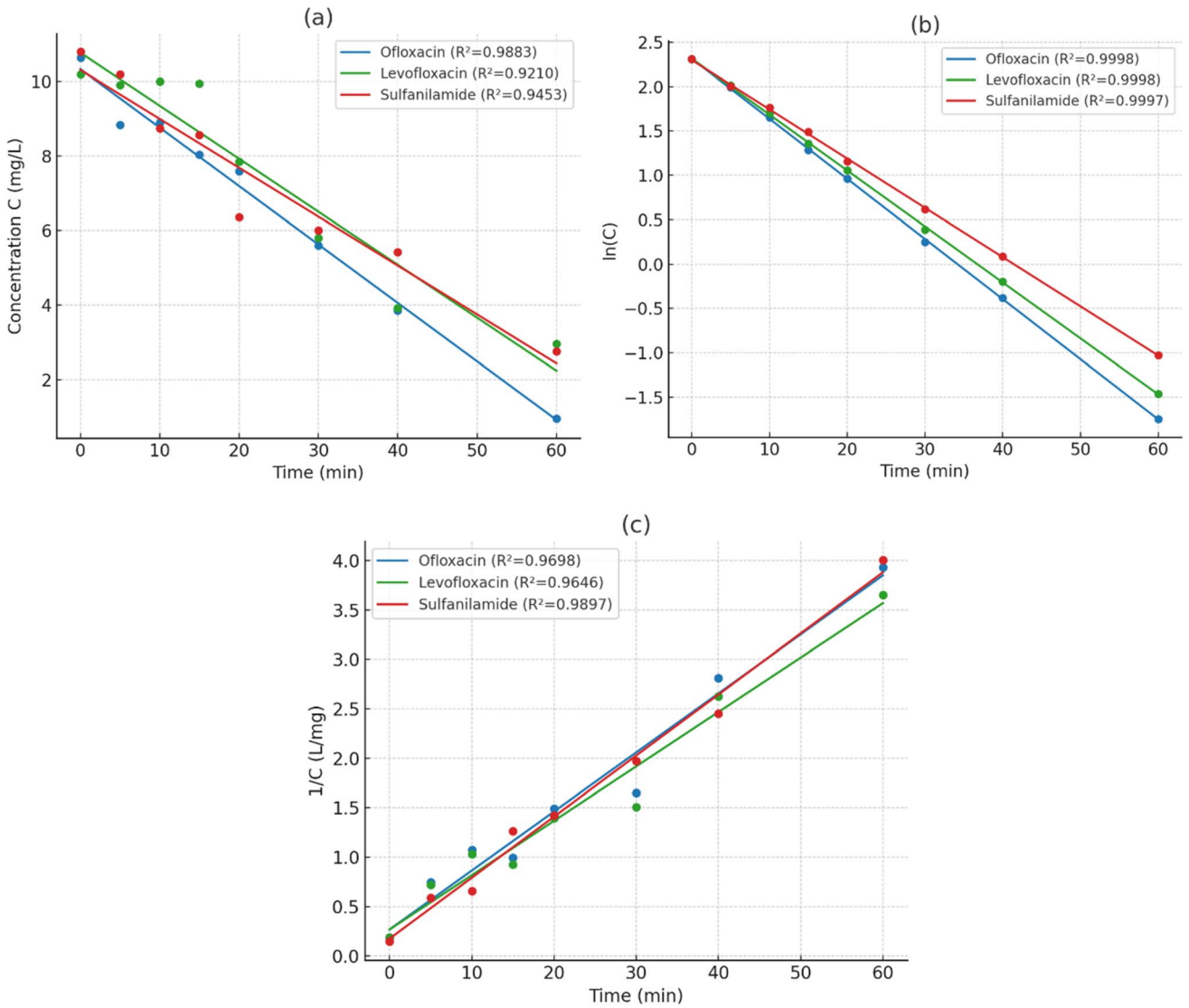

Fig. 6 Kinetic model of the degradation of ofloxacin (OFL), levofloxacin (LEVO) and sulfanilamide (SFA) by $CuMnO_2$@CoPc/Ti foam/UV/PS: (a) zero order; (b) first order; (c) second order.

model was the most suitable for all three compounds. Specifically, the correlation coefficients reached $R^2 = 0.9997–0.9998$, which was superior to the remaining models (Fig. 6b). The linear regression line for ln(C) *versus* time shows that the antibiotic degradation reaction follows the equation:

$$\ln(C_t) = \ln(C_o) - k_{app}t$$

From there, the apparent reaction rate coefficient k_{app} was determined from the slope of the trendline. This is a common feature of advanced oxidation processes (AOPs) involving free radicals ($^{\bullet}OH$, $SO_4^{\bullet-}$), which follow assumed first-order kinetics because the concentration of the oxidant (PS or free radical) is much larger than that of the initial substrate. According to Oturan & Aaron,[48] free radical-mediated oxidation reactions mostly follow an assumed first-order mechanism because the concentration of the oxidant remains almost constant throughout the process. Compared with other studies, this result is consistent with Milh *et al.*[13] when studying the degradation of ciprofloxacin (CIP) in the UV/PS and UV/PMS systems, in which both processes exhibited a strong fit to a pseudo-first-order kinetic model. Chen *et al.*[49] also reported first-order kinetics for the degradation of sulfamethoxazole in the sunlight/Fe(II)/Cit/PS system, with k values of ~0.0363 min^{-1} at room temperature. In this study, the k_{app} values were determined to be 0.0426 ± 0.0015 $hours^{-1}$ (OFL), 0.0410 ± 0.0017 $hours^{-1}$ (LEVO), and 0.0393 ± 0.0013 $minutes^{-1}$ (SFA), and the corresponding semi-automatic values were 16.3, 16.9, and 17.6 minutes.

In contrast, the zero- and second-order models had significantly lower R^2 coefficients (0.92–0.98), indicating that the reaction did not proceed at a linear rate in C (zero-order) or $1/C$ (second-order). Specifically: With the zero-order model (Fig. 6a), the reaction was assumed to be independent of the initial concentration, which is not consistent with experimental observations, especially at low concentrations. The second-order model (Fig. 6c) – commonly seen in co-catalysis – shows a clear deviation at long times, which may be due to strong adsorption at the catalyst surface or free radical competition.

In summary, the assumed first-order kinetic model best reflects the degradation of OFL, LEVO and SFA on the $CuMnO_2$@CoPc/Ti foam catalyst under UV/PS. This is the basis for further calculations of kinetic parameters such as activation energy (E_a) and rate coefficients in future studies.

3.2.2. Effect of UV/PS on antibiotic degradation efficiency. In the treatment system of wastewater containing antibiotics, the presence of oxidizing agents such as PS (persulfate) and UV light plays a very important role in activating and generating highly active free radicals, especially sulfate ($SO_4^{\bullet-}$) and hydroxyl ($^{\bullet}OH$) radicals. In this section, the degradation efficiencies of three representative compounds, ofloxacin (OFL), levofloxacin (LEVO), and sulfanilamide (SFA), were evaluated under different conditions: without UV and PS, only UV, only PS, combined UV/PS, and UV/PS with $CuMnO_2$@CoPc/Ti foam catalyst (Fig. 7). This comparison aims to determine the actual role of each agent and the corresponding activation mechanism. The experimental results show that under the condition without any catalyst or activator, the three antibiotic

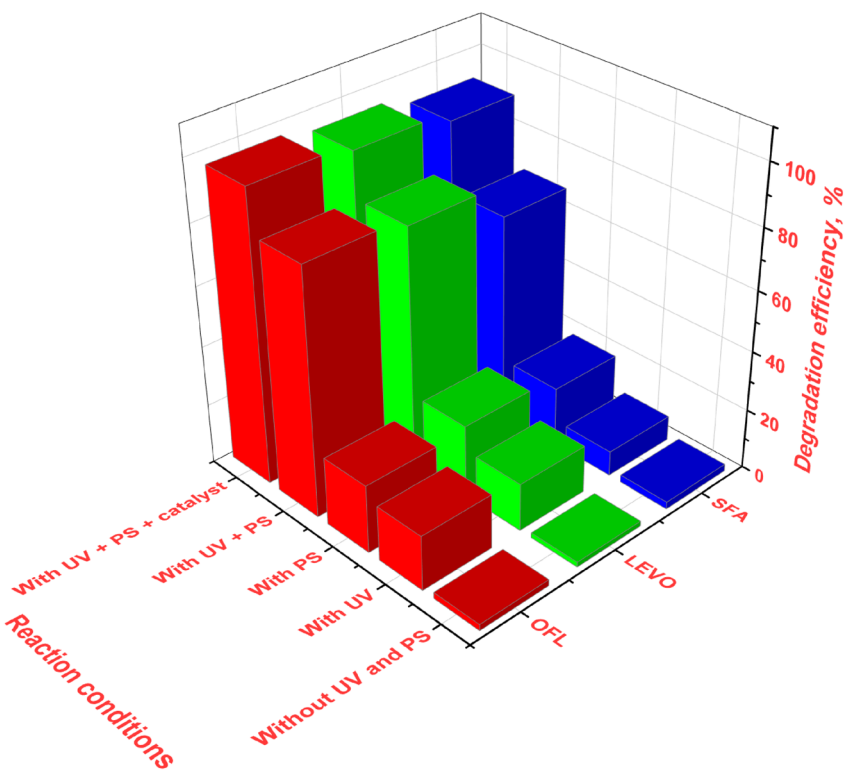

Fig. 7 Effect of UV/PS on the degradation of ofloxacin (OFL), levofloxacin (LEVO) and sulfanilamide (SFA) by $CuMnO_2$@CoPc/Ti foam.

compounds all have very low degradation efficiencies, usually below 5% after 60 minutes of reaction. This shows that the above compounds have high molecular stability under natural conditions and cannot be degraded biologically or physically in a short time.

When exposed to a single 365 nm UV light, the degradation efficiency improved but was still limited. Specifically, OFL achieved an efficiency of about 18.4%, LEVO was 15.9%, while SFA only achieved 8.3%. This reflects the difference in UV absorption capacity and molecular structure of each compound. Fluoroquinolone compounds such as OFL and LEVO have better UV light absorption capacity due to the aromatic ring with conjugated double bonds and attached fluorine atoms, thereby leading to a higher direct photolysis process.[50] However, this process is still not strong enough to completely break the bonds in the molecular structure.

The addition of PS without UV irradiation increased the degradation efficiency to 19–25%, due to the spontaneous decomposition of PS in an aqueous environment to produce $SO_4^{\bullet -}$ radicals. However, this reaction was slow and inefficient without a catalyst or external activation energy source. Compared to the study by Liu *et al.*,[51] in which PS was used to treat SFA, the degradation efficiency was about 0% after 60 min without UV, UV irradiation significantly boosted the efficiency of sulfanilamide decomposition by PS, achieving 72.6% within 60 minutes, indicating the need for PS activation to accelerate the reaction.

When UV was combined with PS, the degradation efficiency of all three compounds increased significantly. OFL and LEVO reached 82.3% and 79.5% after 60 min, respectively, while SFA reached 68.4%. The mechanism of PS activation by UV leads to the cleavage of the O–O bond in $S_2O_8^{2-}$ to generate strong oxidants such as $SO_4^{\bullet -}$ and $^{\bullet}OH$.

$$S_2O_8^{2-} + h\nu\ (\lambda = 254\ \text{nm}) \rightarrow 2SO_4^{\bullet -}$$

$$SO_4^{\bullet -} + H_2O \rightarrow {}^{\bullet}OH + HSO_4^{-}$$

These radicals have very high oxidation potentials, strong enough to break the C–N, C–F and C–S bonds in the antibiotic structure.

What is particularly remarkable is that when adding the $CuMnO_2$@CoPc/Ti foam catalyst to the UV/PS system, the degradation efficiency is clearly superior. Specifically, OFL reached 96.8%, LEVO reached 94.5%, and SFA also reached 91.3% after only 30 minutes of reaction. This increase in efficiency is explained by the catalytic role of the Cu^{2+}/Cu^{+} and Mn^{3+}/Mn^{2+} redox pairs in the activation of persulfate.

$$Cu^{2+} + S_2O_8^{2-} \rightarrow Cu^{+} + SO_4^{\bullet -} + SO_4^{2-}$$

$$Mn^{3+} + S_2O_8^{2-} \rightarrow Mn^{2+} + SO_4^{\bullet -} + SO_4^{2-}$$

In addition, the CoPc layer acts as an electron carrier, reducing free radical recombination and supporting light energy conversion, enhancing the efficiency of heterogeneous catalysis.

Experimental results show that the UV/PS system with $CuMnO_2$@CoPc/Ti foam can decompose over 90% of OFL, LEVO and SFA compounds after only 60 minutes of reaction. This confirms the synergistic effect between UV light, persulfate and catalytic materials in creating strong oxidants and decomposing stable antibiotic compounds in the aquatic environment.

3.2.3. Effect of pH. pH is one of the most important factors affecting the degradation efficiency of organic pollutants in advanced oxidation reaction (AOP) systems, especially when using PS and transition metal catalysts. In this study, three typical pH values were investigated, namely pH 4.0 (weakly acidic environment), pH 7.0 (neutral) and pH 9.0 (slightly alkaline), to evaluate the effect of pH on the treatment ability of three antibiotic compounds OFL, LEVO and SFA in the $CuMnO_2$@CoPc/Ti foam system combined with UV/PS (Fig. 8). The experimental results showed that the highest degradation efficiency was achieved at pH 4.0 for all three investigated compounds. Specifically, the treatment efficiency of OFL reached 98.2%, LEVO reached 96.7%, and SFA reached 93.5% after only 30 minutes of reaction. When the reaction was switched to neutral medium (pH 7.0), the yield dropped to about 90–93% for OFL and LEVO, and 85% for SFA. At alkaline medium (pH 9.0), the yield continued to decline significantly, reaching only about 78–82% for OFL and LEVO, and below 70% for SFA. This significant difference in reaction yield reflects the strong influence of pH on the PS activation mechanism and the survival of the oxidant radicals.

The PS reaction mechanism in acidic medium is more favorable because HSO_5^{-} can be catalyzed or irradiated to form $SO_4^{\bullet -}$ radicals with high yield. The $SO_4^{\bullet -}$ radical has a high oxidation potential (2.5–3.1 V), is stable in acidic solutions, and readily reacts with organics *via* an electron-attack mechanism. Meanwhile, in alkaline environment, HSO_5^{-} is easily decomposed into SO_4^{2-} and cannot form highly active free radicals. In addition, $SO_4^{\bullet -}$ at high pH is also converted into weaker $OH^{\bullet}$ radicals, reducing the overall decomposition efficiency. These phenomena have been demonstrated in the work of Kemmou

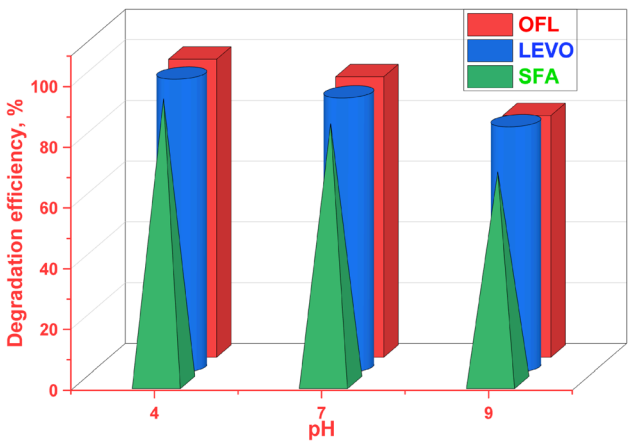

Fig. 8 Effect of pH on the degradation of ofloxacin (OFL), levofloxacin (LEVO) and sulfanilamide (SFA) by $CuMnO_2$@CoPc/Ti foam/UV/PS.

et al.,[52] when treating sulfamethoxazole by biochar-activated persulfate, the decomposition efficiency decreased as the pH increased from acidic to near-neutral and then to alkaline conditions.

In addition, pH affects the ionization state of antibiotic compounds in solution. Compounds such as OFL and LEVO have pK_a in the range of 5.5–6.5, so at pH 4, they mainly exist in the protonated form. This increases the ability to interact with the negatively charged catalyst surface, thereby improving the initial adsorption efficiency – an important prerequisite for the oxidation reaction. In contrast, at high pH, most of the molecules exist in the anionic or neutral form, reducing the adsorption capacity due to the electrostatic repulsion between the catalyst surface and the pollutant. SFA was more strongly affected, due to its molecular structure with less conjugated aromatic rings, so its reaction with oxidant radicals was also lower in alkaline environments. These results are consistent with the study of Jiang *et al.*,[53] in which the ZVI/BC/PS system treated atrazine with an efficiency of 68% at pH 3 but only 46% at pH 8 after the same reaction time.

From the above analysis, it can be concluded that the environmental pH has a significant influence on the efficiency of antibiotic treatment by the $CuMnO_2$@CoPc/Ti foam/UV/PS system, and the most optimal condition is in a slightly acidic environment (pH ~4). This conclusion has practical value in the design and adjustment of pharmaceutical wastewater treatment systems, especially in the pretreatment stage or neutralization of the influent pH to maximize the efficiency of pollutant removal.

3.2.4. Effect of temperature. Reaction temperature is an important parameter in advanced oxidation processes, affecting not only the chemical reaction rate but also the molecular kinetics, the adsorption of pollutants on the catalyst surface and the degradation of oxidizing agents such as PS. In this study, the degradation efficiencies of three representative antibiotic compounds – ofloxacin (OFL), levofloxacin (LEVO) and sulfanilamide (SFA) – were investigated at different temperatures: 20 °C, 30 °C, 40 °C and 50 °C (Fig. 9). The experiments were carried out under fixed reaction conditions of pH, PS concentration, catalyst mass and UV irradiation intensity, in order to evaluate the effect of temperature separately. The results showed that the degradation efficiencies of all three compounds increased gradually with the increase of temperature. At 20 °C, the degradation efficiency of OFL was 81.4%, LEVO was 77.8% and SFA was only 69.2% after 30 minutes of reaction. When the temperature increased to 30 °C, the respective yields of these compounds were 87.2%, 84.1% and 76.3%, respectively. At 40 °C, the yields continued to improve significantly, with OFL reaching 93.5%, LEVO reaching 91.2% and SFA reaching 86.4%. Most notably, at 50 °C, the reaction system reached its maximum efficiency in the study, with values of 97.3%, 95.6% and 91.7% for OFL, LEVO and SFA, respectively. This demonstrates that temperature plays a strong supporting role in the degradation process, especially for structurally stable compounds such as sulfanilamide.

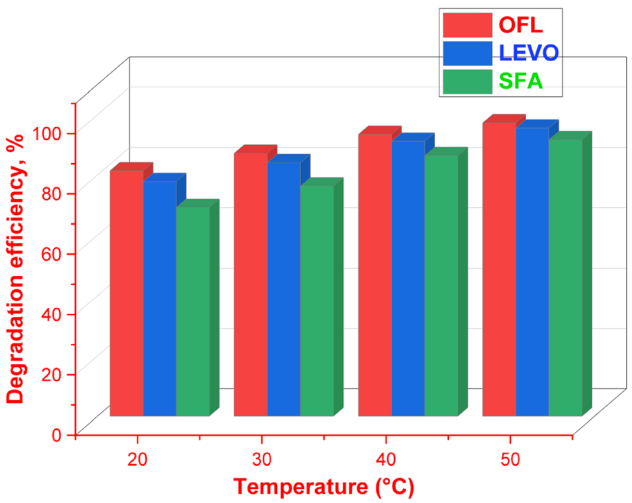

Fig. 9 Effect of temperature on the degradation of ofloxacin (OFL), levofloxacin (LEVO) and sulfanilamide (SFA) by $CuMnO_2$@CoPc/Ti foam/UV/PS.

The mechanism of temperature impact on treatment efficiency can be explained in three aspects. First, according to the Arrhenius law, high temperature increases the average energy of molecules in the reaction system, thereby increasing the probability of effective collisions and promoting the reaction rate between the oxidant radical and the antibiotic molecule. Second, high temperature supports the decomposition of PS to form $SO_4^{\bullet-}$ radicals without completely depending on UV irradiation or catalyst, thereby increasing the density of free radicals in the solution. Third, temperature also increases the diffusion and adsorption rate of antibiotics onto the catalyst surface, shortening the required contact time and improving the surface reaction efficiency. These results are consistent with the observation from the study of Ma *et al.*,[54] in which the treatment of ciprofloxacin by US/E/PS system also showed that increasing the reaction temperature significantly improved ciprofloxacin removal. However, it should be noted that excessive temperature increase can cause undesirable effects. Specifically, PS can decompose rapidly at high temperatures without generating effective oxidizing radicals, leading to the formation of products such as SO_4^{2-}, HSO_4^- or O_2 – substances that are not strong oxidizing agents. At the same time, high temperatures also increase the rate of self-decomposition of $SO_4^{\bullet-}$ and $^{\bullet}OH$ radicals, reducing the lifetime of these radicals in the solution, thereby affecting the overall treatment efficiency if the optimal temperature threshold is exceeded.

3.2.5. Effect of PS concentration. In the advanced oxidation treatment system using persulfate (PS), the concentration of PS is a factor that directly determines the density of free radicals generated in the solution, thereby affecting the pollutant degradation efficiency. Determining the appropriate PS concentration is important from both technical and economic aspects, because too little PS will not provide enough oxidant radicals to perform the reaction, while too much PS can lead to self-scavenging effect or unnecessary chemical waste. In this study, the effect of PS concentration was investigated in the range of 0.1 to 3.0 mM to evaluate the degradation efficiency of three antibiotic compounds: ofloxacin (OFL), levofloxacin (LEVO) and sulfanilamide (SFA) (Fig. 10). The experimental

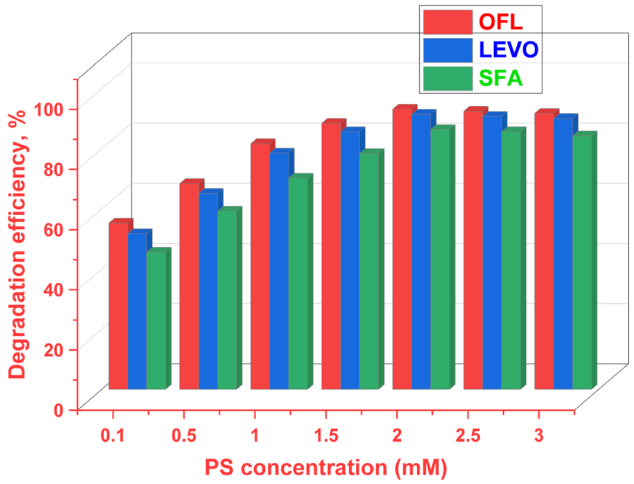

Fig. 10 Effect of PS concentration on the degradation of ofloxacin (OFL), levofloxacin (LEVO) and sulfanilamide (SFA) by $CuMnO_2$@CoPc/Ti foam/UV/PS.

results showed that when the PS concentration increased from 0.1 mM to 2.0 mM, the treatment efficiency of all three compounds increased nearly linearly. Specifically, at a PS concentration of 0.1 mM, the degradation efficiencies of OFL, LEVO and SFA were 55.3%, 51.8% and 45.6%, respectively. When PS was increased to 1.0 mM, the efficiencies improved significantly with values reaching 81.7%, 78.6% and 70.2%. In particular, at a concentration of 2.0 mM, the efficiencies reached a maximum with OFL reaching 93.2%, LEVO reaching 91.5% and SFA reaching 86.4%. However, when the PS concentration was further increased to 2.5 mM and 3.0 mM, the efficiencies did not increase further, and even decreased slightly to 92.5% and 91.8% for OFL, and a similar decrease was observed for the other two compounds. This result suggests that there is an optimal PS concentration, exceeding which may cause an inhibitory effect on the reaction or generate inactive by-products.

The decrease in yield at high PS concentrations is explained by the competitive reactions between PS molecules and the $SO_4^{\bullet-}$ radicals themselves. When the PS concentration is too high, the $SO_4^{\bullet-}$ radicals may react undesirably with excess PS to form less active radicals or even unreacted products, according to the equation:

$$SO_4^{\bullet-} + S_2O_8^{2-} \rightarrow SO_5^{\bullet-} + SO_4^{2-}$$

The $SO_5^{\bullet-}$ radical has been shown to have a significantly lower oxidation potential than $SO_4^{\bullet-}$, and is incapable of breaking the strong bonds in antibiotic molecules. Furthermore, the $SO_4^{\bullet-}$ radical can also react with each other to form neutral SO_4^{2-}:

$$SO_4^{\bullet-} + SO_4^{\bullet-} \rightarrow S_2O_8^{2-}$$

These reactions reduce the concentration of active radicals in the solution and lead to a decrease in reaction efficiency.

In addition, PS is a strong oxidant, when present at high concentrations, it can also damage the catalyst structure or cause aging of the catalyst surface through excessive oxidation, reducing the adsorption capacity and promoting subsequent reactions. A similar phenomenon was also observed in the study by Dong *et al.*,[55] where an excess amount of PS in the Fe(II)/PS system caused a sharp decrease in iopamidol (IPM) treatment efficiency, likely due to the scavenging of oxidative radicals by the excess persulfate (PS).

From the obtained data, it can be determined that the optimal PS concentration for the $CuMnO_2$@CoPc/UV/PS reaction system is about 2.0 mM. This is the level that gives the highest treatment efficiency without causing side effects, which is in line with the practical operational requirements of chemical costs and environmental safety.

3.2.6. Effect of initial concentration of the pollutant. The initial concentration of the pollutant, in this case the three antibiotic compounds ofloxacin (OFL), levofloxacin (LEVO) and sulfanilamide (SFA), is one of the important factors affecting the treatment efficiency and reaction kinetics of the advanced oxidation system. The investigation of this factor not only helps to understand the operational limits of the catalytic system but also helps to determine the scalability and practical application for the treatment of wastewater with different pollutant loads. In this study, the initial concentrations of the compounds were adjusted at the levels: 5, 10, 15 and 20 mg L^{-1}, keeping the remaining conditions unchanged including: pH = 4, temperature = 30 °C, PS = 2.0 mM, catalyst mass = 0.3 g L^{-1}, UV irradiation 365 nm power 30 W (Fig. 11). The experiments were carried out for 30 minutes, measuring the degradation efficiency by UV-vis spectroscopy. The results showed that as the initial antibiotic concentration increased, the degradation efficiency of the catalytic system gradually decreased for all three investigated compounds. At the lowest concentration (5 mg L^{-1}), the degradation efficiency was high: OFL was 98.3%, LEVO was 96.5% and SFA was 91.2%. When the initial concentration increased to 10 mg L^{-1}, the efficiency remained

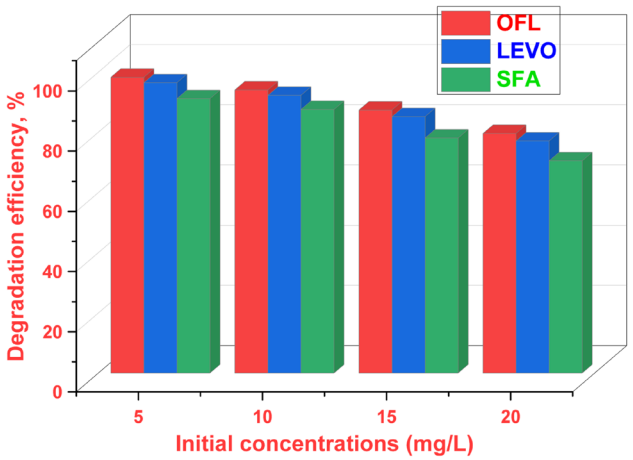

Fig. 11 Effect of initial concentration on the degradation of ofloxacin (OFL), levofloxacin (LEVO) and sulfanilamide (SFA) by $CuMnO_2$@CoPc/Ti foam/UV/PS.

at a good level, with OFL reaching 94.1%, LEVO 92.3% and SFA 87.6%. However, at 15 mg L^{-1}, the efficiency dropped significantly to about 87.4%, 85.2% and 78.1% for the three substances, respectively. In particular, at the highest concentration of 20 mg L^{-1}, the efficiency dropped sharply to 79.6% with OFL, 77.1% with LEVO and only 70.5% with SFA. The main reason for this phenomenon is explained by the fact that the density of oxidant radicals generated in the solution is relatively fixed according to the concentration of PS and catalyst. When the concentration of the pollutant increases, the number of antibiotic molecules increases but there is no corresponding increase in the number of $SO_4^{\bullet-}$ or $^{\bullet}OH$ radicals, leading to the phenomenon of reaction overload. In addition, a large amount of pollutants also increases the probability of competitive reactions with intermediates or half-degradation products, consuming free radicals without contributing to the main reaction. This phenomenon is also known as "quenching" of oxidant radicals. This result is consistent with previous studies. In the work of by Al-Musawi *et al.*,[56] when treating levofloxacin with the MWCNTs/$CoFe_2O_4$ system, the degradation efficiency decreased by nearly 23% when increasing the antibiotic concentration from 50 to 100 mg L^{-1}. From a kinetic perspective, increasing the initial concentration can change the dominant reaction mechanism from pseudo-first-order kinetics to higher-order kinetics due to the significant role of adsorption. When the catalyst surface is saturated with pollutant molecules, the reaction rate is no longer linearly proportional to the initial concentration but is governed by the phenomenon of desorption and the ability to propagate free radicals to the reaction site.

3.2.7. Effect of catalyst mass. Catalyst mass is a key factor in heterogeneous reaction systems, playing a decisive role in the pollutant adsorption capacity and the activation level of oxidants. In the $CuMnO_2$@CoPc/UV/PS system, the catalyst is not only the place to generate free radicals such as $SO_4^{\bullet-}$ and $^{\bullet}OH$ from PS molecules but also the adsorption center that helps concentrate antibiotics into the effective reaction zone. Therefore, investigating the influence of catalyst mass will provide practical information to optimize the treatment system in terms of both efficiency and economy. In this study, the catalyst mass was varied in the range of 0.1 g L^{-1} to 0.5 g L^{-1}, with the reaction conditions kept the same: PS concentration 2.0 mM, pH = 4, temperature 30 °C, UV irradiation power 30 W and influent pollutant concentration of 10 mg L^{-1} (Fig. 12). The results were evaluated after 30 minutes of reaction by absorption spectroscopy. The experimental results showed that the decomposition efficiency increased significantly when the catalyst mass increased from 0.1 to 0.3 g L^{-1}. Specifically, at 0.1 g L^{-1}, the treatment efficiencies of OFL, LEVO and SFA were 78.2%, 74.6% and 69.1%, respectively. When the catalyst amount was increased to 0.2 g L^{-1}, the efficiency improved significantly to 88.3%, 85.9% and 80.5%. The strongest increase was observed at 0.3 g L^{-1}, with values of 94.6%, 92.8% and 87.4% for OFL, LEVO and SFA, respectively. However, when the catalyst amount continued to increase to 0.4 and 0.5 g L^{-1}, the efficiency only increased insignificantly, even tended to be saturated and decreased slightly. This suggests that there is an optimal catalyst loading, beyond which no corresponding improvement in treatment efficiency will be achieved.

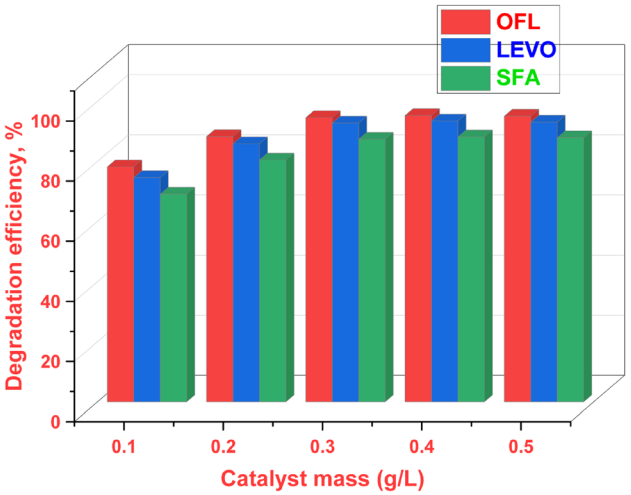

Fig. 12 Effect of catalyst mass on the degradation of ofloxacin (OFL), levofloxacin (LEVO) and sulfanilamide (SFA) by $CuMnO_2$@CoPc/Ti foam/UV/PS.

The phenomenon of performance saturation with increasing catalyst loading has been explained by many previous studies. On the one hand, as the catalyst loading increases, the active surface area and the number of catalyst sites also increase, leading to higher PS activation and pollutant adsorption. However, when the catalyst loading is too high, the catalyst particles tend to aggregate together (agglomeration), reducing the total actual contact area. At the same time, excess catalyst can also lead to inefficient consumption of free radicals through side reactions such as:

$$SO_4^{\bullet-} + M^{n+} \rightarrow M^{n++} + SO_4^{2-}$$

In which, M^{n+} is the active metal ion in the catalyst crystal lattice such as Cu^{2+} or Mn^{3+}. These reactions do not produce the desired product and reduce the density of $SO_4^{\bullet-}$ radicals in the solution. In addition, the excess catalyst layer in the suspension can hinder the transmission of UV light, reducing the efficiency of PS activation in deep regions of the solution, as demonstrated in the study of Marinho *et al.*[57]

3.3. Reaction mechanism of the degradation of pollutants by $CuMnO_2$@CoPc/Ti foam

The XPS spectra provide a consistent and convincing surface picture of the persulfate activation mechanism on $CuMnO_2$@CoPc/Ti foam. In the Cu 2p region (Fig. S1a and Table S1.1), the coexistence of Cu^+ ($2p_3/_2 \approx 932.4$ eV; $2p_1/_2 \approx 952.2$ eV) and Cu^{2+} ($2p_3/_2 \approx 934.6$ eV; $2p_1/_2 \approx 954.3$ eV) and the characteristic shake-up bands at ~941–945 and ~962–965 eV confirm the surface-active Cu(I)/Cu(II) redox couple. The Cu^{2+}/Cu^+ area ratio remains almost constant after five cycles (from 61/39 → 60/40), with no significant binding energy shift, implying that the Cu sites are not reduced/solvated and are efficiently regenerated during the reaction. At Mn 2p (Fig. S1b and Table S1.2), the two

pairs of Mn^{3+} (≈641.8/653.4 eV) and Mn^{4+} (≈643.5/654.9 eV) peaks overlap in the familiar multiplet splitting pattern; the Mn^{4+}/Mn^{3+} ratio only varies from 55/45 to 54/46, indicating that Mn(III)/Mn(IV) cycling occurs but the overall electronic balance is maintained. For Co 2p (Fig. S1c and Table S1.3), the two states Co(II) (≈780.8/797.1 eV) and Co(III) (≈779.6/795.8 eV) and the satellites ~786–789 and ~803–806 eV retain their shape and amplitude after cycling (Co^{2+}/Co^{3+} 53/47 → 54/46), indicating that the CoPc motif is not demetallated or coordinately changed under UV/PS conditions. The O 1s spectrum (Fig. S1d and Table S1.4) splits into $O_{lattice}$ (~529.6 eV), $O_{defect/OH}$ (~531.2 eV) and O_{ads} (~532.4 eV) with a nearly conserved percentage distribution (approximately 52/36/12 → 51/37/12). The slight increase in $O_{defect/OH}$ shows that the defect/hydroxyl centers – which are "hot spots" for adsorption and electron transfer – not only do not disappear but are also maintained after many cycles.

From these XPS observations, the mechanism can be described as follows. Under UV irradiation, CoPc absorbs light to form an excited state CoPc* as a local electron/hole source:

$$\mathrm{CoPc} + h\nu \rightarrow \mathrm{CoPc}^*$$

$$\mathrm{CoPc}^* \rightarrow \mathrm{CoPc}^{\bullet+} + \mathrm{e}^-$$

Photogenerated electrons are injected to transition metal pairs on $CuMnO_2$, rapidly re-reducing the higher oxidation states:

$$\mathrm{Cu}^{2+} + \mathrm{e}^- \rightarrow \mathrm{Cu}^+$$

$$\mathrm{Mn}^{4+} + \mathrm{e}^- \rightarrow \mathrm{Mn}^{3+}$$

$$\mathrm{Co}^{3+} + \mathrm{e}^- \rightarrow \mathrm{Co}^{2+}$$

In the opposite direction, low-valence states activate persulfate *via* surface electron transfer to generate sulfate radicals:

$$\mathrm{S_2O_8^{2-}} + \mathrm{e}^- \rightarrow \mathrm{SO_4^{\bullet-}} + \mathrm{SO_4^{2-}}$$

$$\mathrm{Cu^+/Mn^{3+}/Co^{2+}} + \mathrm{S_2O_8^{2-}} \rightarrow \mathrm{Cu^{2+}/Mn^{4+}/Co^{3+}} + \mathrm{SO_4^{\bullet-}} + \mathrm{SO_4^{2-}}$$

The $SO_4^{\bullet-}$ radical can be further converted to $^{\bullet}OH$ in water, expanding the spectrum of oxidizing agents:

$$\mathrm{SO_4^{\bullet-}} + \mathrm{H_2O} \rightarrow {}^{\bullet}\mathrm{OH} + \mathrm{HSO_4^-}$$

The role of surface oxygen is evident in O 1s: $O_{lattice}$ provides a stable M–O–M framework, while $O_{defect/OH}$ anchors persulfate and contaminants, lowering the electron transfer barrier; these defects are also the site of formation of active species near the surface. The conservation of the oxygen structure (no BE shift, stable distribution) is consistent with the fact that the Cu/Mn/Co redox pairs maintain the same ratio after cycling, meaning that the heterojunction is capable of self-recharging electrons: electrons from CoPc* and organic intermediates continuously close the cycles Cu(I) ↔ Cu(II), Mn(III) ↔ Mn(IV), Co(II) ↔ Co(III), while persulfate $SO_4^{\bullet-}/{}^{\bullet}OH$ to mineralize the substrate. This "role assignment" – CoPc captures light and donates electrons, Cu/Mn/Co serves as the polycentric PS activation site, O_{defect} assists in adsorption and electron transfer – explains why the peak shapes and valence ratios remain nearly constant over multiple cycles, and is consistent with the observed stable degradation efficiency and high mineralization. In other words, XPS not only confirms the surface composition and valence, but also provides direct evidence that the UV/PS mechanism in this system is based on a cooperative redox network that is stable over time.

The EPR data directly demonstrated the free radical mechanism of the UV/PS system with $CuMnO_2$@CoPc/Ti foam and quantified the contribution of each active agent. In H_2O with DMPO (50 mM), the DMPO–$^{\bullet}OH$ spectrum appeared immediately with a 1 : 2 : 2 : 1 tetralinear pattern, $g \approx 2.005$ and $a_N \approx a_H \approx 14.9$ G; while in 50% MeOH/H_2O to stabilize the sulfate adduct, the DMPO–$SO_4^{\bullet-}$ spectrum clearly showed a hexagonal pattern (triplet × doublet) with $g \approx 2.006$, $a_N \approx 13.2$ G and $a_H \approx 9.6$ G (Fig. S2a, S2b and Table S2). All signals disappeared in the no UV/no PS/no catalyst controls, confirming that radicals are only generated when all three factors are present. Radical quenching experiments showed that 0.5 M TBA strongly reduced the $^{\bullet}OH$ signal (~72 ± 3%), 1.0 M MeOH also suppressed both $SO_4^{\bullet-}/{}^{\bullet}OH$ (~85 ± 4%), while 20 mM NaN_3 had almost no effect (<8%), ruling out a dominant role for $^1O_2$. Combining radical quenching with the quadratic integration of the EPR spectrum, the estimated relative contributions were $SO_4^{\bullet-} = 58 \pm 6\%$, $^{\bullet}OH = 34 \pm 5\%$, others ≤ 8% (Table S2). The time course (0–120 s) shows that the EPR intensity increases rapidly in the first 20–40 s and then reaches near equilibrium, consistent with the continuous activation of PS on the heterojunction surface (Fig. S2c). Depending on the concentration, PS exhibits a saturation pattern with a maximum at 2.0 mM and a slight decrease at 2.5–3.0 mM (Fig. S2d), possibly due to the "self-quenching"/radical capture reaction by excess PS and radical recombination: $SO_4^{\bullet-} + S_2O_8^{2-} \rightarrow SO_4^{2-} + S_2O_8^{\bullet-}$ (forming less active radicals) and $SO_4^{\bullet-} + SO_4^{\bullet-} \rightarrow S_2O_8^{2-}$. These observations are consistent with XPS: the Cu(II)/Cu(I) and Mn(IV)/Mn(III) pairs (along with Co(III)/Co(II) of CoPc) remained almost unchanged after five cycles, indicating that the sustained redox cycling on the surface is the PS activator.

The UV-vis DRS spectrum shows that the $CuMnO_2$@CoPc/Ti foam sample absorbs more strongly and broadly than $CuMnO_2$, with the characteristic bands of CoPc (shoulder at ~340 nm and "Q-bands" at ~610–690 nm) overlapping the absorption background of $CuMnO_2$; the absorption edges are clearly red-shifted and the overall intensity increases (Fig. S3a). The Kubelka–Munk transform $F(R) = (1-R)^2/(2R)$ combined with the Tauc plot $[F(R)\cdot h\nu]^{1/2} - h\nu$ allows extrapolation of the linear region to determine the optical band gap. The results show that the apparent E_g of $CuMnO_2$ ≈ 1.41 eV, decreases to ≈ 1.31 eV for $CuMnO_2$@CoPc (fresh sample) and remains almost unchanged after 5 cycles (≈1.32 eV), demonstrating the optical stability of the CoPc layer (Fig. S3b). The narrowing of E_g ~0.10 eV together with the appearance/emphasis of the Soret–Q bands of CoPc indicate that CoPc acts as a photosensitizer, creating additional effective electron–hole transition channels in the visible region.

Mechanistically, under illumination excited states of CoPc (CoPc*) form and transfer electrons across the interface to the acceptor ($CuMnO_2$ or directly to persulfate), while the remaining holes on CoPc/$CuMnO_2$ oxidize water/–OH. This increases the excited carrier density and explains the resonance with persulfate activation. The "red shift" of the absorption edge and the smaller apparent E_g may also reflect the IFCT/Urbach tail transition at the CoPc–$CuMnO_2$ interface, which is commonly observed in phthalocyanine/oxide systems and induces a "light-induced electron conduction" effect in the lower energy region. On the other hand, the fact that the two Tauc curves of the fresh and after 5 cycles samples are almost identical indicates no degradation or photoabsorption peeling after reuse—consistent with XPS (Cu^{2+}/Cu^{+}, Mn^{4+}/Mn^{3+}, Co^{3+}/Co^{2+} ratios are almost preserved) and EPR ($SO_4^{\bullet-}$ radical intensity is dominant, optimal at PS = 2.0 mM).

3.4. Degradation pathways of pollutants

3.4.1. Ofloxacin (OFL) degradation pathway. The degradation mechanism of ofloxacin (OFL) in the $CuMnO_2$@cobalt phthalocyanine heterogeneous photocatalytic system immobilized on titanium foam (Ti foam) under UV irradiation and the presence of persulfate (PS) was elucidated through the combination of LC-MS/MS analysis and total organic carbon (TOC) monitoring. The results showed that OFL (m/z = 362) was degraded *via* four main pathways, each leading to the formation of intermediate products with significantly lower m/z values, reflecting the gradual breakdown of the molecular structure (Fig. 13).

In the first pathway, the OFL molecule is attacked by strong free radicals such as $SO_4^{\bullet-}$ or $^{\bullet}OH$ generated from the activation of PS under the action of the catalyst, leading to quinolone ring opening and the formation of product P1 (m/z = 305). The ring system was then further cleaved to form P2 (m/z = 279) and finally P3 (m/z = 168), indicating a deep and comprehensive mineralization of the quinolone structure. This ring opening mechanism is similar to that reported in the $CoFe_2O_4$/PS catalyst system by Fan *et al.*, in which the quinolone ring was also considered to be a vulnerable starting point due to the high electron density near the carbonyl position.[58] The second

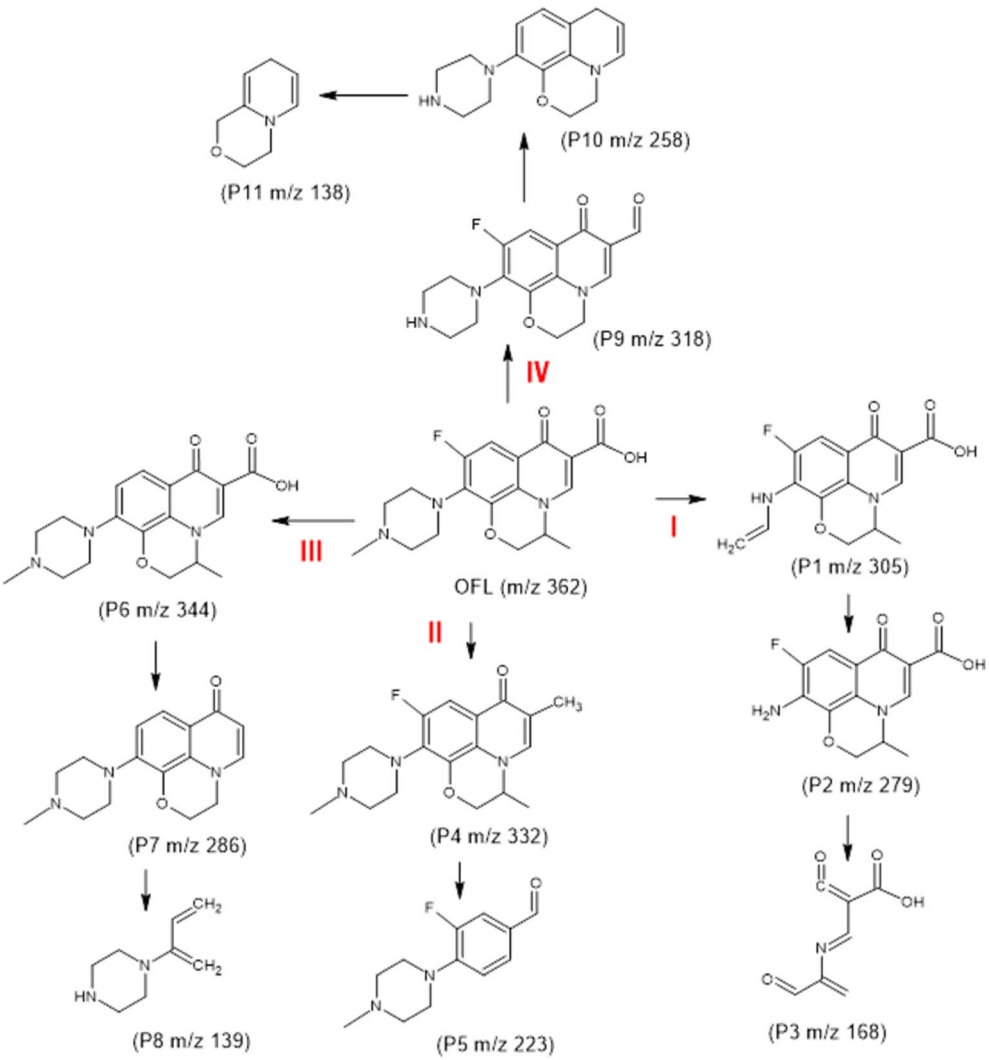

Fig. 13 Possible degradation pathways of OFL by $CuMnO_2$@CoPc/Ti foam/UV/PS.

pathway was reported to involve the reduction of the carboxylic group (–COOH) to a methyl group ($–CH_3$), reducing the molecular weight to $m/z = 332$ (P4). The free radicals then further cleaved the single rings – especially the piperazinyl ring – to form product P5 ($m/z = 223$). Compared with the mechanism reported by Liu *et al.* reported that during the UV/PS treatment of ofloxacin, decarboxylation is one of the characteristic pathways in the initial detoxification process and a precursor to further destruction.[59] The third pathway begins with the removal of the fluorine (F) atom from the aromatic position, forming P6 ($m/z = 344$). This is a common reaction in fluoroquinolone treatment, since the F atom, although stable, is easily replaced by the $SO_4^{\bullet-}$ radical under transition metal catalytic conditions. Next, the COOH group is removed to form P7 ($m/z = 286$), and the remaining single rings are broken, forming P8 ($m/z = 139$). The F and COOH elimination mechanism was previously observed in the UV/PDS system by Zhu *et al.*, and was found to be the pathway that significantly reduced the biological activity of OFL.[60] The fourth pathway involves the loss of peripheral methyl groups, typically from the piperazinyl ring and aromatic substituents, leading to intermediate P9 ($m/z = 318$). This is followed by the combined loss of F and COOH to form P10 ($m/z = 258$), before the remaining rings are completely oxidized, resulting in P11 ($m/z = 138$). This process clearly demonstrates the preference of the free radical system to attack easily oxidizable groups before completely destroying the ring framework. This result is consistent with the observation of Xing *et al.* when treating ofloxacin by magnetic $CuFe_2O_4$ coupled PMS system, in which the removal of the methyl group of the piperazinyl substituent was noted to be the initial step for the radical degradation.[61]

In addition to determining the degradation pathways *via* LC-MS/MS, TOC analysis was used to assess the overall mineralization level of the system. The results showed that the TOC concentration decreased from 8.62 mg L^{-1} initially to 2.65 mg L^{-1} after 60 minutes of UV irradiation, corresponding to a mineralization efficiency of 69.3% (Table 2). This is direct evidence of not only the destruction of the chemical structure but also the conversion to CO_2 and H_2O, which significantly reduces the risk of bioresidues of the antibiotic in the aquatic environment.

3.4.2. Mechanism of levofloxacin (LEVO) degradation. The degradation mechanism of levofloxacin (LEVO) in the same heterogeneous photocatalytic system $CuMnO_2$@cobalt phthalocyanine immobilized on titanium foam under UV irradiation and in the presence of persulfate (PS) was investigated based on LC-MS/MS data and the degree of mineralization was evaluated by TOC analysis. As a stereoisomer of ofloxacin, LEVO has a similar chemical structure but exists only as the L-enantiomer, which affects its spatial orientation and ability to react with free radicals. However, the main degradation pathways of LEVO still bear many similarities to those of OFL, with characteristic m/z intermediates and sequential transformations of important functional groups (Fig. 14).

Table 2 TOC values over time in the UV/PS/$CuMnO_2$@CoPc/Ti foam system with OFL

Time (min)	TOC (mg L^{-1})	Degree of mineralization (%)
0	8.62	0
15	6.98	19.1
30	4.87	43.5
45	3.56	58.7
60	2.65	69.3

The levofloxacin molecule ($m/z = 362$) is oxidized *via* $SO_4^{\bullet-}$ and $^{\bullet}OH$ radical reactions, generating at least four main degradation pathways. In the first pathway, the free radical attacks the C=C double bond at position 2–3 of the quinolone ring, causing ring opening and forming intermediate product L1 ($m/z = 305$). This process continues with the cleavage of C–C, C–N bonds in the open ring system, leading to L2 ($m/z = 279$), and finally L3 ($m/z = 168$) – a small, highly polar product, representing the complete destruction of the quinolone ring framework. This mechanism was previously described in the study of Liu *et al.* when treating LEVO with a Eu_2O_3/Co_3O_4 NSs/PMS system, where the quinolone nucleus was identified as the starting point of the reaction due to the high electron density at the π-bonding sites.[62] The second pathway involves the reduction of the carboxylic acid group to a methyl group under free radical conditions, forming L4 ($m/z = 332$). The loss of this polar group makes the molecule more susceptible to attack by $SO_4^{\bullet-}$, especially at the piperazinyl ring, leading to ring cleavage and the formation of L5 ($m/z = 223$). This process reflects the common reactivity of fluoroquinolones, where the –COOH group not only plays a biological role but is also a target of advanced oxidation. The third pathway begins with the removal of a fluorine atom from the aromatic ring, forming L6 ($m/z = 344$). The fluorine atom plays a role in stabilizing the quinolone ring, but under catalytic conditions rich in oxygen radicals, it is easily replaced by a hydroxyl or hydrogen group. The carboxyl group is then removed, forming L7 ($m/z = 286$), and then the remaining rings are broken down, leading to product L8 ($m/z = 139$). The final products often contain phenol, aldehyde, or simple acid groups, indicating that the catalyst system is capable of comprehensively breaking down the original structure. The defluorination mechanism was also reported in the study of Foti *et al.* on the treatment of levofloxacin by simulated irradiation/PDS system,[63] emphasizing the decisive role of fluorine in directing the reaction. The fourth pathway identified was the loss of peripheral methyl groups from the piperazinyl moiety, leading to L9 ($m/z = 318$). Fluorine and COOH were then further eliminated, forming L10 ($m/z = 258$), and finally L11 ($m/z = 138$), a small molecular product, representing the deep mineralization stage. Such partial ring cleavage indicated that LEVO was destroyed not only at the quinolone nucleus but also at the side chain.

To confirm the deep degradation ability of the catalyst, TOC analysis was performed simultaneously with the reaction. The results showed that TOC decreased from 8.59 mg L^{-1} initially to 2.58 mg L^{-1} after 60 min of reaction, corresponding to a mineralization yield of 69.9%, slightly higher than that of ofloxacin under equivalent conditions (Table 3).

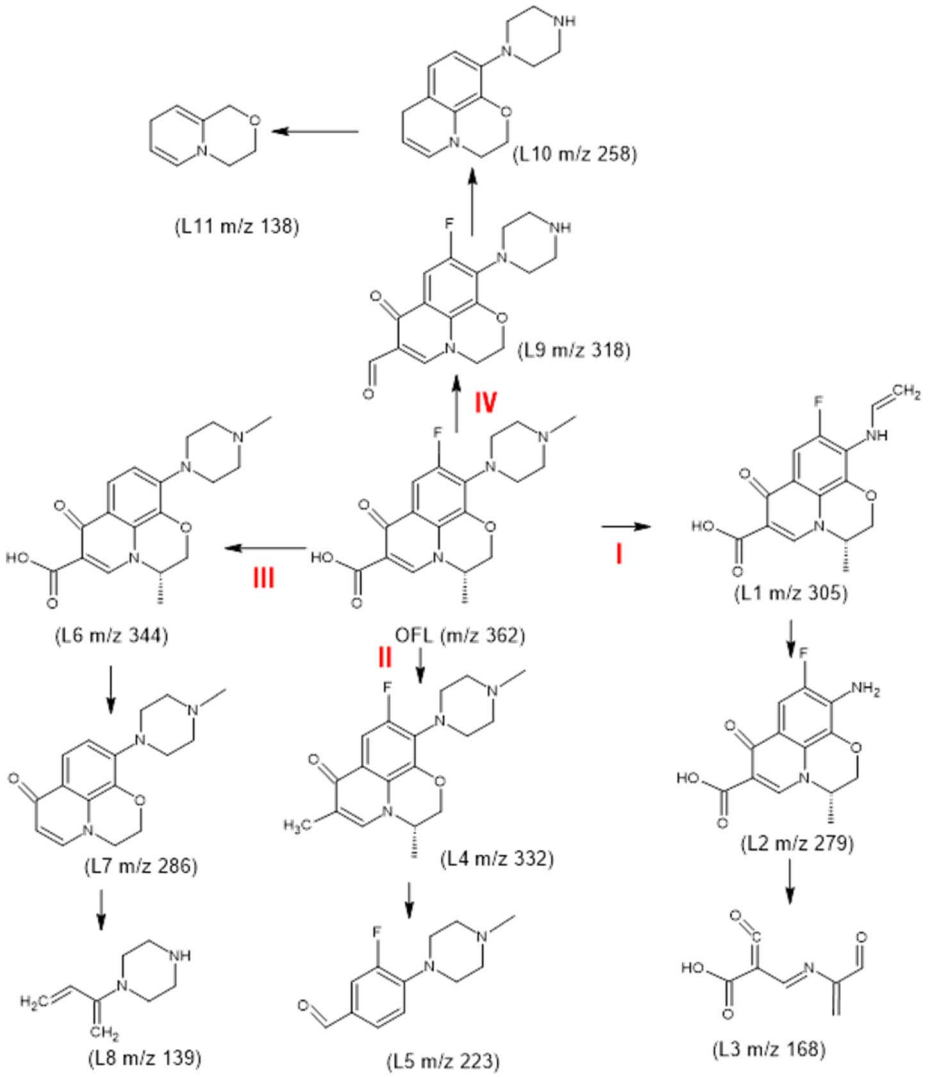

Fig. 14 Possible degradation pathways of LEVO by $CuMnO_2$@CoPc/Ti foam/UV/PS.

3.4.3. Mechanism of sulfanilamide (SFA) degradation. The degradation mechanism of sulfanilamide (SFA) in the heterogeneous $CuMnO_2$@cobalt phthalocyanine catalyst system immobilized on titanium foam under UV irradiation and the presence of persulfate (PS) was determined through LC-MS/MS analysis and the mineralization degree was evaluated by TOC index. Sulfanilamide, a sulfonamide antibiotic, has a simpler structure than ofloxacin or levofloxacin, with a benzene ring attached to a sulfonamide group ($-SO_2NH_2$) at the para position and an aromatic amine group ($-NH_2$). However, the sulfonamide and aromatic amine bonds in the molecule are quite stable under normal conditions, requiring a catalyst system with the ability to generate strong oxidant radicals for effective destruction. Under the action of UV/PS/$CuMnO_2$@CoPc/Ti system, the original SFA molecule (m/z = 172) underwent oxidation of the sulfonamide radical. The NH_2 radical of the $-SO_2NH_2$ group was transformed into the sulfonic hydroxyl group $-SO_2OH$, forming the intermediate product F1 (m/z = 173). This is a typical transformation process that occurs when the $SO_4^{\bullet-}$ radical attacks the nitrogen atom, replacing the NH_2 group with –OH through a simultaneous hydrolysis-oxidation mechanism.[64] F1 can then decompose in two directions. In the first direction, the $-SO_2OH$ group is cleaved, losing the sulfonic chain and leaving the benzene ring, forming F2 (m/z = 93). The second pathway is the decomposition of the remaining $-NH_2$ group of the molecule, forming F3 (m/z = 158), indicating that the free radical attack is not limited to the sulfonamide group but also affects the aromatic amine group (Fig. 15).

Table 3 TOC values over time in the UV/PS/$CuMnO_2$@CoPc/Ti system with LEVO

Time (min)	TOC (mg L^{-1})	Degree of mineralization (%)
0	8.59	0
15	6.85	20.3
30	4.92	42.7
45	3.51	59.1
60	2.58	69.9

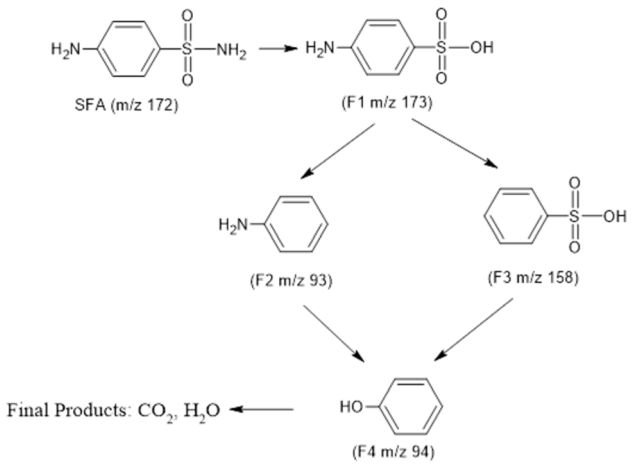

Fig. 15 Possible degradation pathways of SFA by $CuMnO_2$@CoPc/Ti foam/UV/PS.

The convergence of the two pathways is the intermediate product F4 ($m/z = 94$), which can be formed from both F2 and F3. F4 is a small molecule, representing a simplified structure of a strongly modified aromatic ring, possibly a derivative of hydroxylated benzoic acid or simple oxidized aromatic amines. Once formed, F4 is further degraded through free radical oxidation reactions, including carbon chain cleavage and substituent removal, forming small organic acids such as formic acid, acetic acid, and finally CO_2 and H_2O – indicative of complete mineralization.

The TOC results obtained under the same reaction conditions (SFA 10 mg L^{-1}, PS 2.0 mM, catalyst 0.5 g L^{-1}, UV 365 nm) showed that the initial TOC concentration of 7.86 mg L^{-1} decreased to 2.21 mg L^{-1} after 60 min, achieving a mineralization yield of 71.9% (Table 4). The TOC reduction trend showed that the decomposition process was steady and efficient, without the accumulation of stable intermediate products.

3.5. Durability and reusability of catalyst system

Reusability is one of the most important criteria to evaluate the practical application efficiency of a heterogeneous catalytic system in the treatment of polluted water, especially for stable antibiotic compounds such as ofloxacin (OFL), levofloxacin (LEVO) and sulfanilamide (SFA). In this study, the $CuMnO_2$@cobalt phthalocyanine (CoPc) catalyst system immobilized on titanium foam (Ti foam) was tested for durability through

Table 4 TOC values over time in the UV/PS/$CuMnO_2$@CoPc/Ti system with SFA

Time (min)	TOC (mg L^{-1})	Degree of mineralization (%)
0	7.86	0
15	6.32	19.6
30	4.58	41.7
45	3.29	58.1
60	2.21	71.9

Table 5 TOC mineralization efficiency (%) after reuse cycles of $CuMnO_2$@CoPc/Ti foam

	TOC mineralization efficiency, %		
Cycle	Ofloxacin	Levofloxacin	Sulfanilamide
1	69.3	69.9	71.9
2	69.0	69.2	71.3
3	67.2	68.5	70.1
4	65.3	65.9	68.6
5	**62.4**	**63.2**	**66.9**

consecutive reuse experiments under the same reaction conditions (10 mg per L antibiotic, 2.0 mM PS, UV 365 nm, 0.5 g per L catalyst, 60 min). After each cycle, the catalyst material was gently washed with distilled water and ethanol, dried at 60 °C and continued to be used for the next cycle. The results showed that the TOC mineralization efficiency of the catalyst system decreased very slightly after 5 cycles of use for all three antibiotics (Table 5). Specifically, for ofloxacin, the yield decreased from 69.3% to 62.4%; levofloxacin decreased from 69.9% to 63.2%; and sulfanilamide had the highest stability, with the yield only decreasing from 71.9% to 66.9% after 5 uses. This insignificant difference proves that the catalyst system is capable of maintaining high oxidation activity, less affected by intermediate products or active metal leaching during the reaction.

The above results show that the $CuMnO_2$@CoPc/Ti system has a stable structure and good resistance to leaching. In particular, the higher stability of the catalyst in SFA treatment may originate from the simpler molecular structure of SFA, which generates less intermediate products attached to the catalyst surface compared to fluoroquinolones such as OFL and LEVO. On the contrary, the decomposition of OFL and LEVO may generate some hydroxylated aromatic intermediate products or amino acids, which partially hinder the catalytic surface activity in the following cycles. However, the performance degradation after 5 cycles is below 7%, which shows the durable working ability and wide application of the studied catalyst.

In addition, SEM-EDS analysis after 5 cycles did not show any obvious changes in surface morphology or elemental distribution of Cu, Mn and Co on the titanium support, demonstrating that the active sites were stably fixed in the catalyst network. Phthalocyanine cobalt, thanks to its π–π bond and strong electronic interaction with the metal oxide, was not easily washed away, maintaining its effective PS activation role over many cycles (Fig. 16).

ICP-OES analysis of the post-reaction solution confirmed minimal metal leaching: the leaching concentrations (mg L^{-1}) of the metals from the 1st to the 5th cycles were Cu 0.008 → 0.012, Mn 0.006 → 0.009, and Co 0.004 → 0.006, respectively, equivalent to approximately 40–60 μg g^{-1} catalyst per cycle, demonstrating the strong chemical stability of the catalyst (Table S3).

From the above experimental results and discussions, it can be affirmed that the $CuMnO_2$@CoPc/Ti catalyst system not only has high efficiency in degrading three typical antibiotics

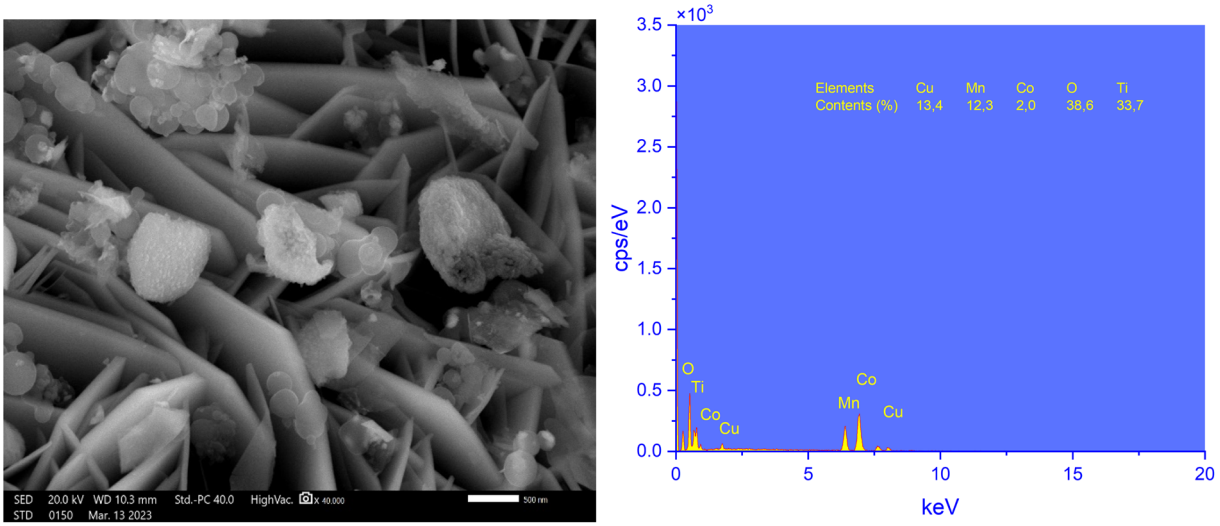

Fig. 16 SEM-EDS analysis of $CuMnO_2$@CoPc/Ti foam/UV/PS after 5 cycles.

representing different structural groups, but also has stable durability and reusability after many reaction cycles. This opens up the potential for wide application of the material in the treatment of wastewater containing antibiotics in hospitals, pharmaceutical factories, or water treatment systems and water reuse in the future.

4 Conclusion

This study demonstrates that a thin, conformal cobalt-phthalocyanine overlayer on crystalline $CuMnO_2$, immobilized as a monolith on Ti foam, creates a robust redox–photosensitizer junction that accelerates UV/PS antibiotic removal. Degradation of ofloxacin, levofloxacin, and sulfanilamide follows pseudo-first-order kinetics with $k_{app} = 0.0426 \pm 0.0015$, 0.0410 ± 0.0017, and 0.0393 ± 0.0013 min^{-1}, respectively, delivering >90% conversion in 60 min accompanied by ~69–72% TOC mineralization. Optical characterization shows that CoPc broadens the absorption envelope and narrows the apparent band gap from ~1.41 to ~1.31 eV, enabling more efficient light harvesting and interfacial charge transfer. Mechanistically, EPR spin-trapping identifies $SO_4^{\bullet-}$ as the dominant oxidant with a secondary $^{\bullet}OH$ contribution, while XPS before/after cycling confirms stable Cu^{2+}/Cu^{+} and Mn^{4+}/Mn^{3+} surface couples and unchanged Co states—evidence that the active redox pairs persist during operation. The monolithic architecture simplifies recovery and resists attrition: activity is retained over at least five cycles, and ICP-OES detects ultra-low metal release (Cu 0.008 → 0.012, Mn 0.006 → 0.009, Co 0.004 → 0.006 mg L^{-1} from cycle 1 → 5; all ≪ 0.1 mg L^{-1}), minimizing secondary contamination risks.

From a process standpoint, the catalyst's durability and separability make it a credible platform for UV/PS polishing of antibiotic-bearing waters. Practical deployment should include residual persulfate quenching (*e.g.*, thiosulfate), sulfate/TDS management, and—where water reuse is targeted—downstream polishing (biologically active filtration and/or activated carbon) plus final disinfection to meet fit-for-purpose quality criteria.

Author contributions

Dinh Ngo Vu: methodology, data curation, formal analysis, and writing – review & editing. Van Chau Dinh: conceptualization, supervision, writing – review & editing. Tien Hoang Nguyen: supervision, writing – review & editing. Phuuoc Cuong Le: data curation, formal analysis. Tan Nhat: conceptualization, methodology, writing – review & editing. Thi Thao Minh: writing – original draft, data curation, formal analysis. Dinh Nhi Bui: writing – original draft, conceptualization, methodology, writing – review & editing, and supervision.

Conflicts of interest

The authors declare that they have no known competing financial interests or personal relationships that could have appeared to influence the work reported in this paper.

Data availability

Data will be made available on request.

Supplementary information is available. See DOI: **https://doi.org/10.1039/d5ra05544j**.

Acknowledgements

This research did not receive any specific grant from funding agencies in the public, commercial, or not-for-profit sectors. We gratefully acknowledge financial support from Electric Power University and Duy Tan University. Portions of the experimental work were carried out at Viet Tri University of Industry, whose laboratory staff we thank for their technical assistance and access to instrumentation.

References

1 A. V. Samrot, S. Wilson, R. S. Sanjay Preeth, P. Prakash, M. Sathiyasree, S. Saigeetha, N. Shobana, S. Pachiyappan and V. V. Rajesh, *Sustainability*, 2023, **15**, 12639.
2 M. P. Gomes, *Water*, 2024, **16**, 2606.
3 P. Välitalo, A. Kruglova, A. Mikola and R. Vahala, *Int. J. Hyg. Environ. Health*, 2017, **220**, 558–569.
4 S. Huang, J. Yu, C. Li, Q. Zhu, Y. Zhang, E. Lichtfouse and N. Marmier, *Water*, 2022, **14**, 3138.
5 V. Homem and L. Santos, *J. Environ. Manage.*, 2011, **92**, 2304–2347.
6 B. Anegbe, I. H. Ifijen, M. Maliki, I. E. Uwidia and A. I. Aigbodion, *Environ. Sci. Eur.*, 2024, **36**, 15.
7 V. R. Keerthika, S. Reshma, M. John, S. Sadhna and J. Eunice, *International Research Journal on Advanced Engineering Hub (also known as IRJAEH)*, 2025, **3**, 330–338.
8 E. M. Cuerda-Correa, M. F. Alexandre-Franco and C. Fernández-González, *Water*, 2019, **12**, 102.
9 J. Wang and R. Zhuan, *Sci. Total Environ.*, 2020, **701**, 135023.
10 S. Li, Y. Wu, H. Zheng, H. Li, Y. Zheng, J. Nan, J. Ma, D. Nagarajan and J.-S. Chang, *Chemosphere*, 2023, **311**, 136977.
11 S. Giannakis, K.-Y. A. Lin and F. Ghanbari, *Chem. Eng. J.*, 2021, **406**, 127083.
12 N. Ali, A. A. Khan, M. Wakeel, I. A. Khan, S. U. Din, S. A. Qaisrani, A. M. Khan and M. U. Hameed, *Water*, 2022, **14**, 3440.
13 H. Milh, X. Yu, D. Cabooter and R. Dewil, *Sci. Total Environ.*, 2021, **764**, 144510.
14 Y. Zhang, L. Li, Z. Pan, Y. Zhu, Y. Shao, Y. Wang and K. Yu, *Chem. Eng. J.*, 2020, **379**, 122354.
15 M. Hasanzadeh, Z. Ghaedrahmat, N. Kayedi, N. J. Haghighi Fard, A. Azari and M. Afsharizadeh, *Heliyon*, 2023, **9**, e21421.
16 D. Manos, K. Miserli and I. Konstantinou, *Catalysts*, 2020, **10**, 1299.
17 N. Akram, J. Guo, W. Ma, Y. Guo, A. Hassan and J. Wang, *Sci. Rep.*, 2020, **10**, 1939.
18 F. Chang, Q. Zhou, H. Pan, X. Liu, H. Zhang, W. Xue and S. Yang, *Energy Technol.*, 2014, **2**, 865–873.
19 A. S. Burange and M. B. Gawande, in *Encyclopedia of Inorganic and Bioinorganic Chemistry*, Wiley, 2016, pp. 1–19.
20 C. Yin, S. Zhou, K. Zhang, J. Bai, Y. Lv, X. Zhang, X. Li and A. Xu, *J. Cleaner Prod.*, 2021, **319**, 128640.
21 L. Zhang, C. Gao, Y. Wang, W. Yu, S. Zhang, B. Zhang and X. Li, *J. Cleaner Prod.*, 2024, **458**, 142517.
22 H. Chen, X. Zhang, Y. Zhao, S. Wang, Y. Ren and X. Wang, *Surf. Interfaces*, 2023, **42**, 103522.
23 S.-H. Wu, J.-L. Wu, S.-Y. Jia, Q.-W. Chang, H.-T. Ren and Y. Liu, *Appl. Surf. Sci.*, 2013, **287**, 389–396.
24 A. E. Pirbazari, *Desalin. Water Treat.*, 2017, **92**, 152–159.
25 S. E. Thoulon, S. Magnin, A. I. Gomes Costa and J. Geringer, *J. Bio- Tribo-Corros.*, 2023, **9**, 49.
26 K. Pałka, R. Pokrowiecki and M. Krzywicka, in *Titanium for Consumer Applications*, Elsevier, 2019, pp. 27–75.
27 B. Xie, Y. Z. Fan, T. Z. Mu and B. Deng, *Mater. Sci. Eng., A*, 2017, **708**, 419–423.
28 Z. Hu, B. Guo, H. Wu, F. Zhu, S. Komarneni and J. Ma, *Colloids Surf., A*, 2022, **654**, 130202.
29 G. Qin, X. Song, Q. Chen, W. He, J. Yang, Y. Li, Y. Zhang, J. Wang and D. D. Dionysiou, *Appl. Catal. B Environ. Energy*, 2024, **344**, 123640.
30 Y. Li, X. Zhang, C. Huang and H. Lyu, *Opt. Mater.*, 2024, **149**, 114994.
31 X. Yang, Q. Jia, J. Pang, Y. Yang, S. Zheng, J. Jia and Z. Qin, *Diamond Relat. Mater.*, 2022, **128**, 109234.
32 H. Zhang, R. Shen, Q. Wang, Y. Hu, L. Niu, Z. Huang, Y. Shao and Z. Wang, *J. Environ. Chem. Eng.*, 2024, **12**, 113230.
33 M. Poienar, A. Lungu, P. Sfirloaga, M. Lungu, C. V. Mihali and P. Vlazan, *Chem. Pap.*, 2019, **73**, 1541–1546.
34 C.-L. Chan, H. K.-F. Wai, P. Wu, S.-W. Lai, O. S.-K. Chan and H. M. Tun, *Antibiotics*, 2022, **11**, 845.
35 C. Cheng, *APL Mater.*, 2023, **11**(7), 1105.
36 S. Durdu, D. Sivlin, K. Ozcan, S. Kalkan, O. Keles and M. Usta, *Sci. Rep.*, 2024, **14**, 618.
37 J. Jia, D. Li, X. Cheng, J. Wan and X. Yu, *Appl. Catal., A*, 2016, **525**, 128–136.
38 S. Campisi, M. Schiavoni, C. Chan-Thaw and A. Villa, *Catalysts*, 2016, **6**, 185.
39 H. R. Barai, N. S. Lopa, F. Ahmed, N. A. Khan, S. A. Ansari, S. W. Joo and Md. M. Rahman, *ACS Omega*, 2020, **5**, 22356–22366.
40 P. A. Sheena, K. P. Priyanka, A. Sreedevi and T. Varghese, *J. Nanostruct. Chem.*, 2018, **8**, 207–215.
41 A. Dauda, A. A. Mahmoud, H. M. Adamu, A. A. Olaleye and A. K. Suleiman, *FUDMA J. Sci.*, 2023, **7**, 275–280.
42 J. O. Rivera-Reyes, K. J. Billings, C. L. Metzler, R. M. Lagle, M. Drabo, R. Palai, J.-P. Jones and D. M. Piñero Cruz, *Chem. Commun.*, 2024, **60**, 4850–4853.
43 X. Huang, C. Ni, G. Zhao and J. T. S. Irvine, *J. Mater. Chem. A*, 2015, **3**, 12958–12964.
44 F. Bahmani, S. H. Kazemi, Y. Wu, L. Liu, Y. Xu and Y. Lei, *Chem. Eng. J.*, 2019, **375**, 121966.
45 S. Zhu, P. Liu and X. Hong, *Nanoscale Adv.*, 2024, **6**, 3211–3219.
46 S. S. Siwal, Q. Zhang, C. Sun and V. K. Thakur, *Nanomaterials*, 2019, **10**, 2.
47 R. Menini, M.-J. Dion, S. K. V. So, M. Gauthier and L.-P. Lefebvre, *J. Electrochem. Soc.*, 2006, **153**, B13.
48 M. A. Oturan and J.-J. Aaron, *Crit. Rev. Environ. Sci. Technol.*, 2014, **44**, 2577–2641.
49 X. Chen, Y. Zhu, Y. Zhou, G. Tang, J. Han and W. Li, *Water*, 2024, **16**, 1564.
50 M. I. Rameel, M. Wali, J. Y. Al-Humaidi, F. Liaqat and M. A. Khan, *Heliyon*, 2023, **9**, e20479.
51 Z. Liu, W. Hu, H. Zhang, H. Wang and P. Sun, *Processes*, 2021, **9**, 226.
52 L. Kemmou, Z. Frontistis, J. Vakros, I. D. Manariotis and D. Mantzavinos, *Catal. Today*, 2018, **313**, 128–133.
53 Z. Jiang, J. Li, D. Jiang, Y. Gao, Y. Chen, W. Wang, B. Cao, Y. Tao, L. Wang and Y. Zhang, *Environ. Res.*, 2020, **184**, 109260.

54 X. Ma and Z. Wang, *Processes*, 2022, **10**, 124.
55 Z. Dong, G. Chen, M. Li, F. Sun, C. Jiang and B. Bharti, *Sci. Rep.*, 2020, **10**, 21548.
56 T. J. Al-Musawi, Y. Q. Almajidi, E. M. Al-Essa, R. M. Romero-Parra, E. R. Alwaily, N. Mengelizadeh, F. Ganji and D. Balarak, *Magnetochemistry*, 2022, **9**, 9.
57 B. A. Marinho, L. Suhadolnik, B. Likozar, M. Huš, Ž. Marinko and M. Čeh, *J. Cleaner Prod.*, 2022, **343**, 131061.
58 Y. Fan, Z. Zhou, Y. Feng, Y. Zhou, L. Wen and K. Shih, *Chem. Eng. J.*, 2020, **383**, 123056.
59 X. Liu, Y. Liu, S. Lu, Z. Wang, Y. Wang, G. Zhang, X. Guo, W. Guo, T. Zhang and B. Xi, *Chem. Eng. J.*, 2020, **385**, 123987.
60 Y. Zhu, M. Wei, Z. Pan, L. Li, J. Liang, K. Yu and Y. Zhang, *Sci. Total Environ.*, 2020, **705**, 135960.
61 C. Xing, K. Chen, L. Hu and L. Liu, *Toxics*, 2024, **12**, 731.
62 J. Liu, Z. Li, M. Wang, C. Jin, J. Kang, Y. Tang and S. Li, *Sep. Purif. Technol.*, 2021, **274**, 118666.
63 L. Foti, D. Coviello, A. Zuorro, F. Lelario, S. A. Bufo, L. Scrano, A. Sauvetre, S. Chiron and M. Brienza, *Environ. Sci. Pollut. Res.*, 2022, **29**, 58201–58211.
64 M. J. García-Galán, M. Silvia Díaz-Cruz and D. Barceló, *TrAC, Trends Anal. Chem.*, 2008, **27**, 1008–1022.